



CHALMERS
UNIVERSITY OF TECHNOLOGY



Using InSAR to detect railway deformations

Master's thesis in Wireless, Photonics and Space Engineering

CARL BERGEVALD

MASTER'S THESIS 2019

Using InSAR to detect railway deformations

CARL BERGEVALD



CHALMERS
UNIVERSITY OF TECHNOLOGY

Department of Space, Earth and Environment
Division of Microwave and Optical Remote Sensing
CHALMERS UNIVERSITY OF TECHNOLOGY
Gothenburg, Sweden 2019

Using InSAR to detect railway deformations

CARL BERGEVALD

© CARL BERGEVALD, 2019.

Supervisors:

Anis Elyouncha, Department of Space, Earth and Environment
Erik Toller, Trafikverket

Examiner:

Leif Eriksson, Department of Space, Earth and Environment

Master's Thesis 2019

Department of Space, Earth and Environment
Division of Microwave and Optical Remote Sensing
Chalmers University of Technology
SE-412 96 Gothenburg
Telephone +46 31 772 1000

Cover: Intensity image of the area between Källered and Lindome made from the temporal mean value of 10 acquisitions. The image is shown in MATLAB and contains modified Copernicus Sentinel-1 data 2019.

Typeset in L^AT_EX

Printed by Chalmers Reproservice
Gothenburg, Sweden 2019

Using InSAR to detect railway deformations
CARL BERGEVALD
Department of Space, Earth and Environment
Chalmers University of Technology

Abstract

Railway deformations are issues that can possibly prevent an effective railway network. Serious deformations may lead to decreased speed limits or in worst case the need for closing parts of the railway for traffic until maintenance work has been performed. The idea is that displacement maps from InSAR images can be used to detect problematic areas so that the right actions could be taken before the deformations become so large that they affect the traffic. Displacement images produced by SkyGeo from the TerraSAR-X satellites have been used by Trafikverket in other projects with good result. The issue is that TerraSAR-X data is expensive so the idea is to use the freely available Sentinel-1 data instead. Displacement maps produced by SkyGeo for both Sentinel-1 and TerraSAR-X, and a displacement map produced by processing in the Sentinel Application Platform (SNAP) over an area south of Gothenburg, Sweden are compared. It was found that using persistent scatterer interferometry on a stack of images alone was not enough to remove enough errors and the results were unreliable. However, when looking at the displacement images provided by SkyGeo which has used models for error reduction, it seemed like the results were more reliable. The results from the Sentinel-1 data had more fluctuations and thus a slightly larger RMS error compared to the results from the TerraSAR-X data but the trends were still clearly visible. A comparison of the coherence and RMS errors showed that there is a connection between high coherence values and low RMS errors which means that where there is high coherence there should also be a low RMS error. The conclusion is that the use of Sentinel-1 data to create displacement maps is plausible and seem to work well in the area used in the project. However, further research on error sources and different nature types in other areas is desired before reliable displacement maps can be made over the entire land mass of Sweden.

Keywords: InSAR, Persistent scatterer, Differential InSAR, Displacement, Sentinel-1, TerraSAR-X.

Acknowledgements

I would like to thank all the people working in the Department of Space, Earth and Environment that has helped me whenever I got stuck with the software or had concerns regarding the theoretical aspects of InSAR processing. I would especially want to thank my supervisors at Chalmers and Trafikverket and my examiner for their help and support throughout the project. Without their help, it would not have been possible to complete this project. I would also like to thank the people at Trafikverket who has helped me extract data from Optram and valuable discussions about soil deformations and how to measure them as well as permission to use the data in the analysis. I would like to thank the European Union, the European Space Agency (ESA) and the Copernicus programme for making the Sentinel-1 data available which enables projects like this. Large thanks to SkyGeo who not only gave me permission to use the previous results but also provided processed Sentinel-1 data so that I could make a more qualitative comparison between the displacement maps from Sentinel-1 and TerraSAR-X. I would also like to thank WSP for the interest in the use of InSAR and for the permission to use the results from the TerraSAR-X data. Last but not least, I am thankful for my family and friends providing me with unlimited support and has never backed away from interesting discussions that has helped greatly in this project and made the last 5 years of my university studies wonderful.

Carl Bergevald, Gothenburg, May 2019

Contents

List of Figures	xi
List of Tables	xv
1 Introduction	1
1.1 Method and aim	1
1.2 Demarcations	2
1.3 Ethical aspects	2
2 Theory	3
2.1 SAR	3
2.2 InSAR	5
2.2.1 Differential InSAR	8
2.2.2 Persistent scatterer interferometry	10
3 Methods	13
3.1 Area selection	13
3.2 Data retrieval	13
3.3 Data processing	15
3.3.1 DInSAR in SNAP toolbox	15
3.3.2 PSI in SNAP toolbox	18
3.4 Processing by SkyGeo	20
3.5 Result analysis	21
3.6 Compare PSI and Optram	23
4 Results	25
4.1 Intensity measurements	25
4.2 DInSAR in SNAP	27
4.3 PSI with TerraSAR-X	29
4.4 PSI in SNAP	33
4.5 PSI with Sentinel-1 by SkyGeo	37
4.6 Optram	45
5 Discussion	47
5.1 DInSAR in SNAP	47
5.2 Sentinel-1 in SNAP compared to results by SkyGeo	49
5.3 TerraSAR-X compared to Sentinel-1	50

5.4	InSAR and Optram	51
5.5	Errors and noise	52
6	Conclusions	53
6.1	Intensity measurement	53
6.2	Differential in SNAP	53
6.3	Persistent scatterer	53

List of Figures

2.1	Overview of the SAR geometry.	4
3.1	Overview of the SLC image as seen from the satellite.	14
3.2	How to get displacement from 5 images. The colors of the brackets correspond to the color of the point in the graph. The black point in the graph denotes the first image, the reference 0 m at day 1.	19
4.1	Intensity averaged from 10 intensity measurements between March and June 2018. The Figure contains modified Copernicus Sentinel-1 data [2019].	26
4.2	Google Earth image over the area (Left) and the intensity image map projected in Google Earth (Right). The Google Earth image shows the train stations and railway (contains modified Copernicus Sentinel-1 data 2019).	26
4.3	Displacement maps of Källered station (Left) and Lindome station (Right) obtained by 2-pass DInSAR with Sentinel-1 data and the SRTM DEM with a temporal baseline of 18 days. The displacement maps are projected in Google Earth.	27
4.4	Coherence values corresponding to the 2-pass DInSAR images of Källered station (Left) and Lindome station (Right). The coherence values are map projected in Google Earth. The Figure contains modified Copernicus Sentinel-1 data [2019].	28
4.5	Displacement maps of Källered station (Left) and Lindome station (Right) obtained by 3-pass DInSAR using Sentinel-1 data.	28
4.6	Coherence values corresponding to the 3-pass DInSAR images of Källered station (Left) and Lindome station (Right). The coherence maps are map projected in Google Earth.	29
4.7	Displacement maps over Lindome station (Left) and Källered station (Right) using TerraSAR-X data. Note that the dots do not represent the pixel size, they show the center of the pixel. The images are courtesy of SkyGeo and used with permission from SkyGeo, WSP and Trafikverket. The data are shown in a map by Bing.	29
4.8	Displacement map over the total area of interest analyzed from TerraSAR-X data. The processing is done by SkyGeo. The image is courtesy of SkyGeo and used with permission from SkyGeo, WSP and Trafikverket. The data is shown in a map by Bing.	30

4.9	Displacement over time for the TerraSAR-X data for a stable point (Top), uplift (Middle), and settlement (Bottom).	31
4.10	Photo of the railway track at Lindome station. It is possible to see how the railway tracks and platform form a slope after the tunnel.	32
4.11	Histogram of the RMS errors in the results from TerraSAR-X.	32
4.12	RMS errors plotted as a function of the coherence of the TerraSAR-X results by SkyGeo.	33
4.13	Coherence maps over time for the area of interest for the Sentinel-1 data.	34
4.14	Coherence plotted for 3 different pixels in the Sentinel-1 data processed in SNAP. Top) A typical bad pixel Middle) A typical good pixel Bottom) A typical railway pixel.	35
4.15	Displacement maps for Lindome station (Left) and Kållerød station (Right) using the Sentinel-1 data processed in SNAP. The map projections are done in Google Earth.	36
4.16	Displacement over time for a stable point (Top), point with uplift (Middle), and point with settlement (Bottom) from the Sentinel-1 data processed in SNAP.	36
4.17	Histogram of the RMS error of the results from the SNAP processing of the Sentinel-1 data.	37
4.18	Displacement maps over Lindome station (Left) and Kållerød station (Right) using Sentinel-1 data processed by SkyGeo. Note that the dots do not represent the pixel size, they show the center of the pixel. The images are courtesy of SkyGeo and used with permission from SkyGeo, WSP and Trafikverket. The data is shown in a map by Bing.	38
4.19	Displacement map over the total area of interest from Sentinel-1 data. The processing is done by SkyGeo. The image is courtesy of SkyGeo and used with permission from SkyGeo, WSP and Trafikverket. The data is shown in a map by Bing.	39
4.20	Displacement over time for a stable point (Top), point with uplift (Middle), and point with settlement (Bottom) from the Sentinel-1 data processed by SkyGeo.	40
4.21	Histogram of the RMS errors from the Sentinel-1 results analyzed by SkyGeo.	40
4.22	RMS errors as a function of coherence of the Sentinel-1 results processed by SkyGeo.	41
4.23	Displacement over time for the same points as in Figure 4.20 but using a shorter stack.	42
4.24	Histogram of the RMS errors from the Sentinel-1 results analyzed by SkyGeo with fewer acquisitions used.	42

4.25	Displacement rates along the tracks at Lindome station from Sentinel-1 by SkyGeo (Top), Sentinel-1 in SNAP (Middle) and TerraSAR-X by SkyGeo (Bottom). The first point is approximately 100 m north of the platform and continues to approximately 100 m south of the platform. The time periods are June 2016 - May 2019 for Sentinel by SkyGeo, January 2016 - September 2018 for TerraSAR-X by SkyGeo and April 2018 - October 2018 for Sentinel in SNAP.	43
4.26	Displacement rates along the tracks at Kållerød station from Sentinel-1 by SkyGeo (Top), Sentinel-1 in SNAP (Middle) and TerraSAR-X by SkyGeo (Bottom). The first point is approximately 100 m north of the platform and continues to approximately 100 m south of the platform. The time periods are June 2016 -May 2019 for Sentinel by SkyGeo, January 2016 - September 2018 for TerraSAR-Xby SkyGeo and April 2018 - October 2018 for Sentinel in SNAP.	44
4.27	Results from Optram plotted in Google Earth. The pins have accurate positions of the track kilometers (turquoise numbers) but the colors inbetween are not perfectly scaled. The data is used by permission from Trafikverket.	45

List of Tables

3.1	Interferogram formation processing parameters. FE stands for Flat Earth.	16
-----	--	----

1

Introduction

To maintain a reliable infrastructure, the railway must maintain good quality. This is extra important in a time when the railway is a popular way of passenger and freight transport. Soil deformations around the railway is an issue that can potentially affect the railway [1]. In order to guarantee a good condition of the railway, the Swedish Transport Administration, Trafikverket, is monitoring the railway for deformations and fixes them when they occur [2]. This is done using sensors mounted on special measurement trains which require time and resources to operate. This means that the tracks are occupied while the measurements are performed which interrupts the traffic.

Therefore, Trafikverket is interested in evaluating complementary methods for monitoring that can lead to more efficient track measurements. One suggestion is using Interferometric Synthetic Aperture Radar (InSAR) for continuous automatic monitoring. InSAR has been used previously in projects by Trafikverket with good results, but in those cases expensive images with high spatial resolution were bought [3]. The idea is to use free and available data from the Sentinel-1 satellites that does not have as good spatial resolution as the previous InSAR data used by Trafikverket.

By using InSAR data for maintenance and cause evaluation, it is possible to monitor large areas for deformations and to find potential problem areas in a cost efficient way. Measurement trains can then be used more efficiently by focusing the measurements to the problem areas. Problem areas can be avoided altogether when new tracks are being planned which further decreases the need for measurement carts and improves the quality of the railway.

1.1 Method and aim

The goal of this project is to evaluate if it is possible to use InSAR with Sentinel-1 data to measure railway deformations. The evaluation is based on *Spatial- and temporal resolution, geographic location, accuracy of geographic location and height measurements, average of height measurements, deviation from average height measurements, Coherence of the InSAR data* and a comparison of 3 different InSAR techniques *2-pass differential, 3-pass differential and persistent scatterer*.

Spatial resolution is the resolution in space, or the pixel size. Temporal resolution

is the time between the measurements. The geographic location can affect the results since some areas give more or at least more stable backscatter than other. This technique may work very well in some areas but not at all in others. It is also important to see if the pixel positioning is accurate or if there is an offset. The average and standard deviation of the height measurements are evaluated to determine the stability of the measurements. The coherence of the InSAR data is a measure of the quality of the data and if a pixel gives similar amounts of backscatter over time. A high coherence is required for the InSAR technique to work [4]. However, the exact coherence value required is difficult to determine beforehand.

1.2 Demarcations

The differential InSAR and persistent scatterer data processing is done in the free software *Sentinel Application Toolbox (SNAP)* developed by the European Space Agency (ESA). Data processed by SkyGeo is also used and a comparison between the data is done.

The railway track between Kållerød and Lindome is used for the measurements. There have been measurements on the track from the previous InSAR measurement so that the result from the different satellites can be compared. The satellite provides an image of a large area around the track which allows for evaluation of measurements of different surfaces: urban, farmlands, forests etc.

1.3 Ethical aspects

Using InSAR images to detect railway deformation does not have any natural ethical issues. The function is good for society since an effective railway system is a positive thing for society. An effective railway can potentially lead to more people choosing the train instead of air travel or taking the car which could have a positive environmental effect.

One potential negative aspect is that there may be people who think that SAR images violate the personal integrity. While it is true that SAR images cover large areas, the spatial resolution is not good enough to distinguish people in the images. The only thing that could possibly be detectable is if someone makes construction work on their property that changes the scattering properties and thus gives a different intensity value of a few pixels. Because such a change would be so small and thus hardly visible at all and the fact that it would not be visible exactly what is built, a SAR image should not be considered an issue for the personal integrity.

2

Theory

This chapter explains the theory of SAR and InSAR and important parameters to keep track of when processing the radar data. The different InSAR techniques *differential* and *persistent scatterer* are described.

2.1 SAR

In general, a larger antenna aperture implies that a higher resolution can be achieved. This comes from how the antenna beam depends on the antenna aperture size. However, the required size quickly becomes ridiculously large when a high resolution is desired, especially for centimeter and longer wavelengths. For space borne systems, it is not reasonable to launch antennas with a diameter of tens or hundreds of meters into space.

A SAR system overcomes this issue by using a synthetic aperture, hence the name Synthetic Aperture Radar. The antennas are placed on a platform moving with a constant velocity while transmitting radar pulses with a certain pulse repetition frequency (PRF) [5]. The receiving antenna is collecting reflected pulses from an object as long as the object lies within the antenna beam, thus the object is observed for some time and not just in an instant, which enables improved resolution [5].

The size of the footprint on the Earth depends on the dimensions of the physical antenna and the wavelength. For a circular antenna with an aperture with diameter D , the beamwidth is determined as λ/D [6]. The SAR geometry is shown in Figure 2.1. This would be the spatial resolution if a snapshot was taken with the system. Because several pulses are used under a longer observing time, the spatial resolution can be improved within the footprint. The whole footprint is still observed but reflections from smaller objects can be distinguished.

The spatial resolution is divided into *Range*- and *Azimuth* resolution. According to [6], the range resolution depends on the pulse length τ which is defined as $1/B$, where B is the bandwidth of the SAR system. The resolution ΔR in slant range is then defined as

$$\Delta R = \frac{C\tau}{2} \tag{2.1}$$

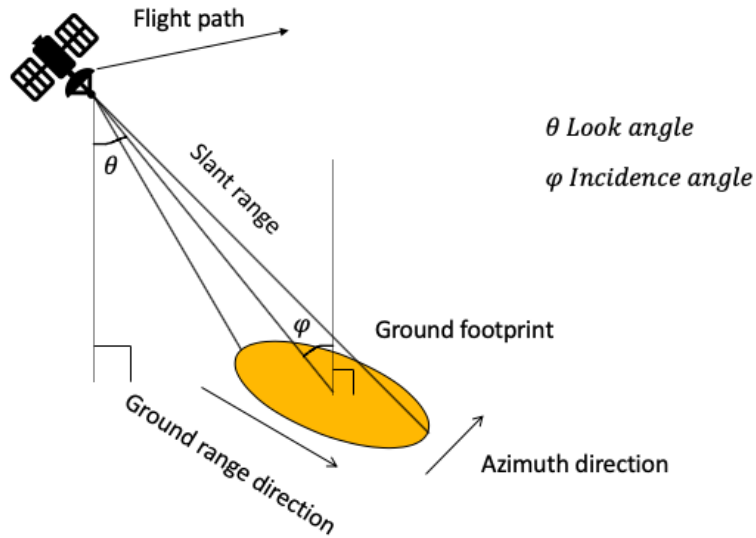


Figure 2.1: Overview of the SAR geometry.

where C is the speed of light in vacuum [6].

However, since the pulse is illuminating the ground with an angle φ , eq. (2.1) describes the resolution in slant range, i.e. the propagation direction of the pulse, and not the resolution on the ground. The range resolution on the ground ΔR_g can be calculated from a ground projection of the slant range using the incidence angle [6].

$$\Delta R_g = \frac{C\tau}{2 \cdot \sin(\varphi)} \quad (2.2)$$

The cross range or azimuth resolution depends on the acquisition mode, but for stripmap mode which is when the antenna beam is at a fixed position looking at a direction perpendicular to the flight direction, the azimuth resolution can be written [6]

$$\Delta R_{az} \approx \frac{\lambda}{2\theta_{3dB}} \quad (2.3)$$

where λ is the wavelength and θ_{3dB} is the 3dB opening angle of the antenna.

The amplitude of the received pulses can be used to create high resolution images of the Earth or other areas of interest. For example, SAR is used to create images of inaccessible places on the Earth. Other land applications are land monitoring and determining the amount of vegetation [7]. Some ocean applications are ice monitoring and detection of oil spills.

One advantage of a SAR system is that it is an active system [5], i.e. the pulses are generated by the system so that the system is not relying on external sources. This enables the system to work at any time as opposed to some passive systems which

require sunlight and thus only work during daytime.

The wavelength is another advantage. SAR systems use radio frequencies which are not sensitive to clouds [5]. This means that SAR images can be taken when there is a cloud layer above the desired area. Different wavelengths are used in different SAR systems depending on the application. The wavelength determines what the system can see. The radar pulses pass right through objects much smaller than the wavelength making the objects invisible in the radar image [5]. This can for example be used in order to select whether or not one wants to see the foliage in forest images. Longer wavelengths goes through the foliage and shorter wavelengths are reflected on it. For some applications it is preferred to see objects below the foliage and then longer wavelengths are more suitable. Most SAR systems operate in a single frequency band, and thus one must select the system that is best used for the application.

2.2 InSAR

Interferometric SAR uses the phase information of the received pulse as opposed to regular SAR that uses the amplitude of the pulse. By using several measurements with a temporal and spatial baseline, i.e. a difference in time and space respectively, the phase difference between the different measurements can be used to create elevation-, and displacement maps [8, 9, 10].

For Sentinel-1, the measuring method is called *repeat-pass interferometry* since the satellite is repeating the orbit and thereby repeating the passage over the area of interest [10]. The temporal- and spatial baselines are thus naturally created by the satellite orbit as it takes a number of days before the orbit repeats and the orbits are not repeated down to meter level. There are two Sentinel-1 satellites, platform A and B. Their orbits are designed to repeat every 12 days and platform B has a 180° orbital shift with respect to the orbit of platform A, enabling a temporal baseline of 6 days if both platforms are used [11].

One important step in the processing of InSAR data is to create an interferogram from 2 images. The interferogram is defined as one image multiplied with the complex conjugate of the other image according to [9, 12]

$$I_{inter} = I_1 * I_2^* \quad (2.4)$$

Note that the * denotes cross multiplication between the images.

Before the interferogram formation is possible, it is important that the location of the images matches each other with great accuracy [13]. The mismatch must be much less than a pixel. Some algorithms can create a mismatch less than 0.001 of a pixel [4, 14]. This is done by coregistration of the images. One is set as a reference, or master image and the other is set as a slave image [13]. The time delay and spatial offset of the slave image is estimated to get an overlap between the images.

I_1 and I_2 in eq. (2.4) are the coregistered images.

The interferogram contains the phase information that is used to create elevation models or displacement maps [8, 9, 10]. Because of the geometry in a SAR system, the measured phase differences are measured in slant range, see Figure 2.1. This can later be projected to horizontal and vertical direction with some uncertainty as the exact displacement in other directions than slant range cannot be known by measuring from one direction. Errors when projecting slant range to vertical direction can be reduced by comparing to measurements from another direction, for example by comparing ascending and descending orbits of the satellite. This increases the complexity of the processing.

The main idea of displacement measurements is to use two different interferograms from data acquired at different times. It is assumed that one interferogram is created with two images acquired close in time so that no displacement can be assumed. Then the phase of that interferogram, ϕ_1 describes the topography only [8]

$$\phi_1 = \phi_{topo} \quad (2.5)$$

Then the second interferogram is created using a temporal baseline such that it can be assumed that there is displacement. The phase of this interferogram can then be written [8]

$$\phi_2 = \phi_{topo} + \phi_{disp} \quad (2.6)$$

where ϕ_{disp} is the phase term caused by displacement. Then the displacement could be retrieved by comparing the interferograms

$$\phi_2 - \phi_1 = \phi_{disp} \quad (2.7)$$

The displacement phase ϕ_{disp} can be written [4, 8, 9]

$$\phi_{disp} = \frac{4\pi}{\lambda}d \quad (2.8)$$

where λ is the wavelength of the pulse and d is the phase difference converted to meters.

This is the core to displacement measurements with InSAR. However, eq. (2.5) and (2.6) are highly simplified and several other contributing phase terms are neglected that will cause a large error term if they are not considered and removed.

According to [4, 9] the phase in the interferogram from repeat-pass measurements consists of

$$\phi = \phi_{flatearth} + \phi_{topo} + \phi_{prop} + \phi_{scat} + \phi_{disp} + \phi_{noise} \quad (2.9)$$

where $\phi_{flatearth}$ is the flat earth phase caused by the fact that the distance to the different pixels varies within the image with respect to a reference system, ϕ_{topo} is the

topographic phase, ϕ_{prop} is the phase difference caused by atmospheric effects, ϕ_{scat} is the phase difference caused by changes in the scatterers that affect the amount of the signal that is reflected back towards the satellite, ϕ_{disp} is the phase related to displacement, and ϕ_{noise} is the noise term. In order to make a good displacement calculation, it is necessary to remove all the other contributions to the phase. It is clear that any remaining errors will directly affect d in eq. (2.8).

The flat earth phase is removed first. Then a phase filter is applied to reduce the amount of phase noise. These steps are done to make the phase unwrapping procedure easier [12].

Phase unwrapping is required because the phase is only measured in one phase cycle, i.e. from $-\pi$ to π radians. This causes a phase ambiguity for phase changes larger than 2π , which is called that the phase is wrapped [8, 9, 12]. This is solved by phase unwrapping which estimates the correct number of phase cycles so that the actual phase difference can be used as ϕ in eq. (2.9) [8, 12].

Another important concept in SAR interferometry is *coherence* and the consequence of decorrelation [8, 9]. In order to create accurate elevation and displacement maps, all pixels should show the same amount of backscatter over time. This ensures that it is the same object that is reflecting the radar pulse. This is important, because if the signal is reflected of different objects, the difference between the objects will give a phase contribution that is misinterpreted as displacement phase. Since the pixels are rather large, approximately 5 m by 20 m in range and azimuth direction respectively [11], it is not only one object that is seen per pixel. Each pixel or resolution cell shows the sum of all contributions within the cell. In this project, the IW (Interferometric Wide swath) mode SLC (Single Look Complex) Sentinel-1 data is used.

In an ideal case, there would be no decorrelation over time but in reality all pixels decorrelate but at different rates. Oceans, lakes, and forest areas decorrelate quickly as water currents and wind causes movement that changes the backscatter [9]. Oceans and lakes often decorrelate so quickly that no result can be found at all. Steady points like buildings and other structures takes much longer to decorrelate and may even stay constant for months or years [15]. These areas are preferred when measuring displacement. It is shown later that the railway gives a strong reflection and that it does not decorrelate quickly. Weather conditions affect the decorrelation as well. Frozen or moist ground changes the backscatter and may cause complete decorrelation with respect to the backscatter of dry ground [16].

A measure of the decorrelation is the coherence of the interferogram. Consider the coregistered images I_1 and I_2 used in eq. (2.4). Each pixel in those images can be written $I_1(m, n)$ and $I_2(m, n)$ respectively, where m is the row index and n is the column index. The estimated coherence $\gamma_{est}(m, n)$ of each pixel can then be written [8]

$$\gamma_{est}(m, n) = \frac{I_1(m, n)I_2^*(m, n)}{\sqrt{I_1^2(m, n)I_2^2(m, n)}} \quad (2.10)$$

It can be noted that when there is a perfect match between $I_1(m, n)$ and $I_2^*(m, n)$, the estimated coherence is 1, and when $I_1(m, n)$ and $I_2^*(m, n)$ are totally decorrelated, the estimated coherence approaches 0. A value close to 1 is desired for high reliability but it is difficult to set a general threshold for when a point is considered unreliable.

The actual value of γ comes from several contributions [8, 12]

$$\gamma = \gamma_{temporal} \cdot \gamma_{geometric} \cdot \gamma_{volumetric} \cdot \gamma_{processing} \quad (2.11)$$

$\gamma_{temporal}$ comes from the decorrelation over time and cannot be removed since it is a natural property of the scattering objects. $\gamma_{geometric}$ comes from differences in the satellite orbit and the effect can be reduced if the errors are treated. $\gamma_{volumetric}$ comes from the vegetation and cannot be removed either since it comes from the property of the scattering objects. $\gamma_{processing}$ should be treated so that no decorrelation is caused by processing errors.

There are several processing techniques for InSAR. The ones that are used in this report are Differential InSAR (DInSAR) and Persistent Scatterer Interferometry (PSI). Both techniques require high coherence for reliable displacement maps. That is a disadvantage as some areas simply cannot give reliable displacement maps because of the natural low coherence. The DInSAR and PSI techniques are described more carefully in sections (2.2.1) and (2.2.2) respectively.

2.2.1 Differential InSAR

DInSAR is a traditional InSAR technique that finds the displacement by subtracting two interferograms similar to eq. (2.7). The phases ϕ_1 and ϕ_2 used for calculating the displacement are processed to remove error sources and reduce uncertainties as much as possible. There are different ways of doing this, but two common methods that are used in this report are 2-pass and 3-pass DInSAR [4]. The names come from how many input images that are required to get a result.

2-pass DInSAR uses data from two passages over the area of interest, i.e. from two images. The images should be taken at times such that there are displacements between them [4]. The images are used to form one interferogram which is the only interferogram that can be created using only two images. This method then requires external data in the form of a digital elevation model (DEM). DEM:s can be created from interferograms containing only the topographic phase information. All other contributions have been removed. DEM:s from InSAR are also projected to show the topography in vertical direction [17] rather than slant range before it can be compared with the measured interferogram [4]. DEM:s can also be created from other types of measurement, for example laser scanning from an airplane which is done by Lantmäteriet in Sweden [18].

There are several DEM:s available. One often used is the SRTM (Shuttle Radar Topography Mission) DEM. The measurement was performed on one of NASA's Space Shuttle missions launched early in year 2000 [19]. It mapped the topography of all land mass on the Earth between latitudes 60° North and 54° South. The

mission was successful and the DEM data with a spatial resolution of 90 meters can be freely downloaded from [20] for small areas at a time. However, one does not usually need more data than for the area of interest.

Although the SRTM DEM is good and widely used in the field of interferometric SAR, it is by no means perfect. There are uncertainties in the DEM that affect the reliability of the measurements [20]. By using many measurements, the uncertainties can be reduced, but since the 2-pass method uses only 2 images, the uncertainty associated with the technique is a drawback.

There are also other DEM:s that can be used. There are authorities or other groups who make land surveys with high accuracy but they are often only measured for small areas and the data is often not freely available. A DEM is not only used in 2-pass DInSAR, it is also used for geocoding the data in most SAR applications.

3-pass DInSAR uses data from three passages which increases the number of options and possible interferograms with different temporal baselines. The images are used to create two interferograms. One of them is used as a DEM while the other contains the displacement. The requirement is that the images used to create the DEM interferogram has a temporal baseline short enough that no movement on the ground can be assumed [4]. The interferograms are created so that they both have the same master image. For example, assume three images I_1 , I_2 and I_3 . Assume that I_1 and I_2 are taken 6 days apart and that no movement can be assumed. Assume that I_3 is taken 24 days after I_2 . I_2 is set as the master and I_1 and I_3 are slave images, coregistered to I_2 . From that, one interferogram is created using I_1 and I_2 . This is considered the DEM as it is assumed to include topography induced phase only. The next interferogram between I_2 and I_3 is then including the topography induced phase and the phase caused by displacement.

3-pass DInSAR has the advantage that creating a DEM with a common master as the next interferogram ensures that movement on the ground has happened during the time period that was observed. When using an external DEM, differences are measured since the DEM was created. However, creating a reliable DEM requires high resolution and high coherence, requirements that may not be met with the Sentinel-1 data [4, 11, 21]. Another theory is that it does not matter since it is the same system that takes all images, so although the errors in this DEM are large they should be present in the next interferogram as well and thus disappear to a large extent when differentiating the interferograms.

2.2.2 Persistent scatterer interferometry

The persistent scatterer (PS) technique is also based on solving eq. (2.7), but the technique is more focused on reducing errors and uncertainties than DInSAR. It is based on the trademarked Permanent Scatterer technique invented by [22], but there are some differences. The idea of the persistent scatterer technique is to build up a stack of many SAR images over long time periods [8]. PSI analysis is done for time series of years to decades including up to 100 images for processing. The idea is that when several images and interferograms are used, errors and uncertainties can be reduced to an extent where displacements in the order of mm/year can be measured accurately [15].

Decorrelation is an issue when working with long time series. As previously mentioned, many objects decorrelate quickly so depending on the area, it may be difficult to find reliable data. The PS technique finds pixels that do not decorrelate quickly. These scattering objects may decorrelate completely over long time periods but appear constant over the time period of the measurements. These are considered stable and persistent, hence the name persistent scatterers [15]. Pixels containing persistent scatterers are the only ones considered in the analysis since only they are considered reliable. The selection of persistent scatterer candidates (PSC) can be done in different ways. One way is to use the coherence values [4, 22]. High coherence implies a stable pixel and all pixels with a coherence value larger than a certain threshold are considered a PSC. The threshold is selected arbitrarily depending on how reliable the results should be and the measured coherence values. High coherence is desired but there is an inevitable trade-off between the number of PSC and a high coherence value. Setting the threshold too high may result in very few PSC, especially in areas that decorrelate quickly. The coherence of a PSC is allowed to decrease as long as it stays above the threshold.

While the coherence thresholding is an easy and effective technique for selecting PSC, [22] mentions some issues. They mention that uncertainties in the DEM and issues when removing the topographic phase may give an erroneous coherence estimation. They propose another method, using the amplitude dispersion index, D_A instead. This method is only statistically accurate when many images are used in the processing. [22] proposes more than 30 images.

D_A is calculated according to

$$D_A \triangleq \frac{\sigma_A}{m_A} \tag{2.12}$$

where σ_A is the standard deviation of the amplitudes of the intensity images and m_A is the mean value of the amplitudes of the intensity images. For example, assume there are 50 SAR images of size $M \times N$. Each amplitude value can be written $A_i(m, n)$, where i denotes the image index ($1 \leq i \leq 50$), m and n are the row- and column indices respectively ($1 \leq m \leq M$, $1 \leq n \leq N$). For each pixel, a stack S is created with amplitude values over time according to

$$\begin{aligned}
S_1 &= [A_1(0,0) \ A_2(0,0) \ \dots \ A_{50}(0,0)] \\
S_2 &= [A_1(0,1) \ A_2(0,1) \ \dots \ A_{50}(0,1)] \\
&\quad \cdot \\
&\quad \cdot \\
S_{M \cdot N} &= [A_1(M,N) \ A_2(M,N) \ \dots \ A_{50}(M,N)]
\end{aligned}$$

D_A for each pixel is then calculated from the mean value and standard deviation of each stack S using eq. (2.12). A stable point has a D_A value approaching 0 as an ideal PSC would have $\sigma_A = 0$. [22] suggests that a reliable PSC should fulfill $D_A < 0.25$.

The large number of images leads to many opportunities for interferograms and baselines. Just like for 3-pass DInSAR, a single master image is selected and all other images are coregistered to that image. The master image should be carefully selected as it will affect the temporal and spatial baselines. If an image in the middle of the time period is selected, the largest temporal baseline is just half of the total period.

Another aspect to consider when selecting the master image is the weather conditions on the dates of the images. Since frost and moisture can decorrelate the images, it is not preferred to select a master image taken on a day with sub-zero temperatures or heavy rain. The best master image from a weather perspective should be taken on a day with neutral weather compared to the other images or a day with dry weather. Slave images taken on a day with bad weather conditions may be accepted as it is often only a few images, if it was the master image it would affect all interferograms. Images taken in snow conditions or frost may sometimes be removed from the stack if they decorrelate the interferograms too much. For example, *InSAR Norway*, which is a Norwegian project to make a nation wide service for displacement maps, uses only measurements during the summer for this reason [23, 24].

The many interferograms in the stack implies that there are several measurements of eq. (2.9). Then instead of approximating values for the different phase contributions and accepting the uncertainties, they can be solved using an iterative algorithm [22]. Although not perfect, the iterative process containing filters and adjustments reduces the uncertainties and errors of the phase contributions. For example DEM errors, orbit parameter errors, and atmospheric delay can be reduced to enable more accurate displacement maps [8, 22]. [22] state that since eq. (2.9) is non-linear, it is not certain that the iterative process converges. They suggest that too large errors in the DEM or any missing baselines in the data set might cause the iterative process to diverge instead.

3

Methods

This chapter explains the selection of the test area, the processing of the InSAR data and the way from retrieving the data from the satellite to a displacement map. It also goes through how the software work.

3.1 Area selection

The area used for the analysis is the railway between Kållerød station and Lindome station south of Gothenburg. This area is selected because it has four important properties.

1. Previous InSAR data exist for this area and can be used for comparison
2. Kållerød and Lindome train stations have known displacement issues that should be detectable
3. The area is easy to visit to make observations in person and get an understanding of how it looks in reality
4. The area has different types of land, for example roads, forests, fields, urban, lakes, etc.

The first and fourth points are especially important because they give an idea of which areas the InSAR technique can be used in and it is easier to evaluate the data if it can be compared to previous results.

3.2 Data retrieval

This section concerning Sentinel-1, its operation and file types is mainly based on [11]. The Sentinel-1 constellation consists of 2 satellites, platform A and B that measure all landmass in the world except for central Antarctica. The two satellites share the same orbit, but are phase shifted 180° in the orbit so that one satellite follows the other. The SAR system on board the satellites is a C-band radar with a frequency of 5.405 GHz and it can measure in 4 different modes. The mode of interest for this to work is the Interferometric Wide swath (IW) mode generating 3 sub-swaths. The antenna beam is steered in azimuth direction so that the same

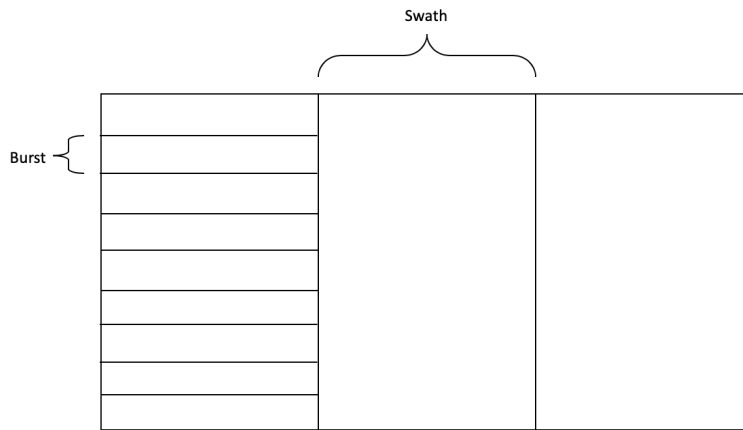


Figure 3.1: Overview of the SLC image as seen from the satellite.

directional antenna gain is experienced for all pixels in the image. This for the cost of slightly reduced azimuth resolution caused by shorter observation time in azimuth compared to having a fixed position of the antenna beam. The antenna beam steering used for IW data is called Terrain Observation with Progressive Scan (TOPS). The TOPS image is divided in 3 sub-swaths which are each divided in 9 bursts. See Figure 3.1. Note that the figure is slightly simplified to create a rectangle. In reality, the swaths may be offset from each other.

The data is transmitted down to Earth and to the European Space Agency (ESA) who operates the satellites. ESA provides the data either as raw data or as pre-processed data. In this project, the Single Look Complex (SLC) format has been used, which is considered a pre-processing version of the raw data. The SLC data is provided in slant range direction and the pre-processing includes georeferencing of the data so that every pixel can be related to a geographical point. This is done by using the orbit data collected by the satellite. ESA uses burst synchronization for the SLC files so that it is possible to coregister the data from different acquisition dates i.e. to enable repeat-pass interferometry.

The data files are made available through the Copernicus portal called Copernicus Open Access hub [25]. There, it is possible to search for desired data over a certain area, acquisition date, measurement mode, and data type. An account is required for downloading the data, but creating an account is free for everyone.

3.3 Data processing

When the data is downloaded it must be processed in order to go from SLC to displacement map. The processing is a complex process but there are various pieces of software available to help. This project uses the freely available Sentinel Application Toolbox (SNAP) software. Because of the large data files and powerful algorithms used for the processing, some processing power is required. Therefore, all processing for this report is done on a server at Chalmers for processing power and available space for the input data.

3.3.1 DInSAR in SNAP toolbox

SNAP is distributed by ESA, just like the SLC data, so many functions are designed to work smoothly with the Sentinel-1 SLC data. SNAP has a graphical user interface that is easy to use and the available functions can be called one at a time or coded into a graph that can execute several functions after each other. There is also the possibility to use the program through bash-scripts and writing the graphs as xml-files.

Both 2-pass and 3-pass DInSAR is performed with SNAP. 2-pass requires 2 SLC images and a DEM. The steps used in the processing are:

1. Coregistration of the SLC images
2. Interferogram formation
3. Deburst
4. Multilooking
5. Phase filtering
6. Phase unwrapping
7. Displacement map formation
8. Geo-correction

Many of these steps have corresponding functions available in SNAP for the Sentinel-1 data. For example, there is a function called *S1 TOPS Coregistration* for the coregistration of the images. In this function, it is possible to select which bursts to include in the coregistration so that unnecessary pixels can be excluded. The input to the function are the master and slave images. The polarization of the signal is also selected in the function. Co-polarization is desired since that gives a higher signal than cross-polarization, and a higher signal is an advantage when creating displacement maps. In this case, Vertical-Vertical polarization is selected. The function uses orbit parameters and a DEM in the process of coregistration. The orbit files and DEM are downloaded automatically through SNAP and there are a few to select from. The orbit files *Sentinel precise* are selected because they are the most accurate for Sentinel, and the SRTM DEM is selected since it is a widely used

DEM. The output of this function is the coregistered slave image.

The next step is the interferogram formation which is done using the function *Interferogram Formation*. The processing parameters includes choices for removing flat earth phase and to remove topographic phase. These are related to eq. (2.9). It is possible to select degree of flat earth polynomial, number of flat earth estimation points, and orbit interpolation degree for the flat earth phase removal algorithm. The selection used for the processing are the recommended values by SNAP and can be found in Table 3.1.

Table 3.1: Interferogram formation processing parameters. FE stands for Flat Earth.

Degree of FE polynomial	5
Number of FE estimation points	501
Orbit interpolation degree	3

In the 2-pass case, it is desired to remove the topographic phase by using a DEM, so the *Remove topographic phase* option is selected and the SRTM DEM is selected.

The last option to consider in the processing parameters is to select to include coherence estimation. Without this option, no coherence values will be given.

Because the coregistration part includes a split so that single bursts can be selected, a function called *S-1 TOPS Deburst* must be used for the coregistered image in order to avoid sections with no or bad data between consecutive bursts or around the edges of the burst.

The interferograms appears to be rather noisy at first. Multilooking and filtering is required in order to remove some of the noise. Multilooking with a factor of 8 in range and 2 in azimuth is applied and SNAP has a function for a Goldstein phase filter which is used to filter the interferogram. After the filtering, the interferogram looks less noisy but the phase is still wrapped and needs to be unwrapped.

There is no unwrapping function built into SNAP, however there is a SNAP extension called SNAPHU (Statistical-Cost, Network-Flow Algorithm for Phase Unwrapping) that performs the phase unwrapping. SNAPHU is created by [26]. A function called *Snaphu Export* prepares for the unwrapping. The processing parameters sets the parameters to be used in the unwrapping algorithm and a directory is created with a configuration file containing the command to write to the SNAPHU program. The unwrapping is executed by running the command from the configuration file in the created SNAPHU-directory using a terminal window. The output of the unwrapping procedure is an .img file used in the function *Snaphu Import* in SNAP in order to read the unwrapped file back into SNAP.

The interferogram, now containing the unwrapped phase does not contain $\phi_{flatearth}$ nor ϕ_{topo} as they have been removed in the interferogram formation. Also the interferogram is filtered so ϕ_{noise} is also removed. Comparing this with eq. (2.9) it can be seen that the phase in the interferogram is

$$\phi = \phi_{disp} + \phi_{prop} + \phi_{scat} + \phi_{error} \quad (3.1)$$

where ϕ_{error} denotes the error terms including remaining flat earth- and topographic phase and phase noise caused by imperfect filtering and removal algorithms. ϕ_{error} is considered as a part of the noise term in eq. (2.9) but is rewritten here as an error when the noise is removed by the filter.

SNAP does not currently have any strong tools for estimation of atmospheric phase and since the coherence is not used, ϕ_{scat} is not considered. Because only 2 images are used and no stack of images, the error parameter cannot be reduced further. Because of this, the assumption is that $\phi_{prop} = \phi_{scat} = \phi_{error} = 0$, meaning that the interferogram phase is only containing the phase difference caused by displacement. While this is not entirely true, there is not much to do about it without adding further assumptions or algorithms outside of SNAP. This must be considered when analyzing the results.

The function *Phase to displacement* is used to convert the phase in the interferogram to a distance. The output of this function is a displacement map in meters showing the displacement in slant range direction and not vertical/horizontal. The vertical/horizontal displacement can be calculated using a projection of the range direction, however this requires an assumption that there is no horizontal displacements. This assumption introduces uncertainties. Therefore, the displacement is kept in slant range direction at this point.

The last step is to perform geo-correction of the data. Up until this point, the images and interferogram has been shown in the way as it is seen from the satellite. While this is the most logical way to process the data, it does not make much sense to look at. Therefore, the function *Range-Doppler Terrain Correction* is used to view the displacement map in map geometry with North-South being up-down and East-West being right-left in the image.

3-pass DInSAR works similar with the difference that similar steps as in 2-pass must be done to create a DEM and then the steps of 2-pass must be done again, but using the created DEM. The steps of 3-pass are:

1. Coregistration of the SLC images that should create DEM
2. Interferogram formation
3. Deburst
4. Multilooking
5. Phase filtering
6. Phase unwrapping
7. DEM formation
8. Geo-correction
9. Save DEM

10. Coregistration of the SLC images that should include displacement
11. Interferogram formation using created DEM
12. Deburst
13. Multilooking
14. Phase filtering
15. Phase unwrapping
16. Displacement map formation
17. Geo-correction

Steps 1-7 describes how to create a DEM from SLC images and steps 8-13 describes how to create a displacement map. Steps 8-13 are the same as 2-pass with the only difference being that when selecting *Remove topographic phase*, instead of SRTM, *External DEM* is selected and the directory to the created DEM is provided.

SNAP supports several outputs but the most important ones are GeoTiff so that the image can be plotted with correct geo-information using an arbitrary software like for example MATLAB, and Kmz format which is Google Earth format which makes it possible to show the image in Google Earth.

3.3.2 PSI in SNAP toolbox

It is not possible to create stacks of images in SNAP and thus a PSI analysis cannot be done completely in SNAP. Instead, several displacement maps similar to a 2-pass differential procedure with corresponding coherence maps are generated in SNAP to be analyzed in MATLAB.

For N measurements where N is an integer value, a displacement map with corresponding coherence is created between images $1 - 2$, $1 - 3$, $1 - 4$, ..., $1 - N$ with the same procedure as 2-pass DInSAR. The differences between PSI and 2-pass DInSAR in this case is that more measurements are used for PSI and that the coherence is considered in PSI. As stated by [22], the PSC selection can be done in different ways. Coherence thresholding combined with intensity thresholding is selected because of the simplicity and effectiveness of the process.

A list of the pixels with a coherence higher than a certain coherence value in interferogram $1 - 2$ is created. All pixels on the list are controlled for all interferograms. If a pixel does not fulfill the threshold criterion, it is removed from the list. When the coherence from all interferograms has been controlled, the list only contains pixels that fulfill the criterion for all interferograms. The pixels on the list are called persistent scatterer candidates or PSC which are the only pixels considered further in the processing. The actual threshold value is selected after observation of the results. Because some pixels that show a strong intensity may show a decreased coherence over time, a low coherence threshold can be accepted for those pixels. However, a pixel with low coherence and low intensity should not be considered a PSC. Intensity

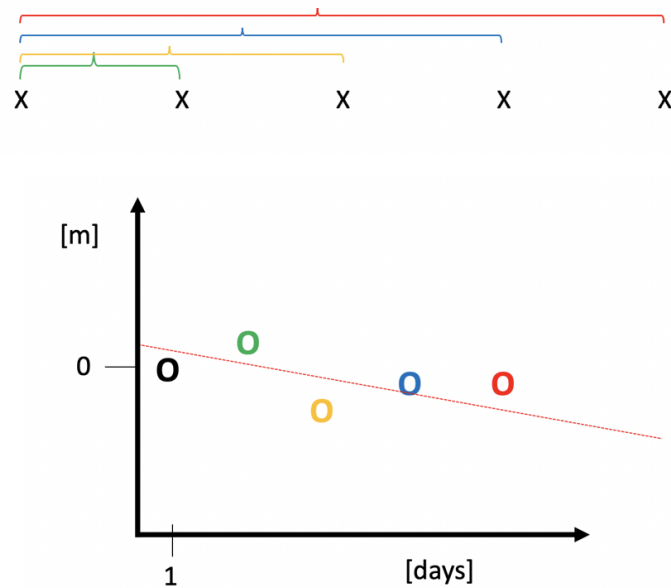


Figure 3.2: How to get displacement from 5 images. The colors of the brackets correspond to the color of the point in the graph. The black point in the graph denotes the first image, the reference 0 m at day 1.

thresholding in this case refers to this kind of intensity consideration. It is difficult to set an absolute intensity threshold, thus a more relative value is used. Pixels with a relatively high intensity value over time are allowed to have lower coherence and still be called PSC as long as they do not decorrelate completely.

The PSC are plotted for displacement over time. This is shown in Figure 3.2. The figure shows how a graph is plotted for 5 images. The first point in the graph is the reference and is set as 0 at measurement day 1. The following points are created from the offset from the reference. When all images are plotted, a linear curve is fitted to the points and the slope of the linear curve gives the displacement rate in m/day, which can easily be converted to mm/year.

Creating other baselines is possible, but increases the difficulty in extracting the displacement referring to the reference point. For example, consider the five measurements in Figure 3.2. If the third measurement is selected as a master, the baselines obtained are $3 - 1$, $3 - 2$, $3 - 4$, and $3 - 5$. It would be possible to obtain the displacement from $1 - 4$ by adding the $1 - 3$ and $3 - 4$ with a correction for the change of sign to turn $3 - 1$ into $1 - 3$. However, the addition adds the errors of each measurement which increases the total errors. Therefore this is not done in this project.

The output from SNAP is the displacement for the different interferograms, the coherence, and the intensity of the images in geotiff format which can be easily read in MATLAB. The first step after reading all the data in MATLAB is to select the PSC. The PSC selection process used is mainly based on coherence thresholding, thus only pixels that has a coherence value larger than a certain threshold value in all interferograms are selected as PSC. An initial test is done for a coherence

threshold of 0.5, but as is shown in the results, the railway decorrelates more in the data so that many railway pixels are excluded for in the PSC selection. As stated by [22], coherence thresholding is not the only way to select PSC. Since the railway shows rather strong backscatter intensity in all the intensity images, a lower coherence threshold is accepted for railway pixels. The new coherence threshold is set to 0.3, but the pixels beside the railway must be treated with caution because if they have both low coherence and show low intensity, they cannot be trusted as PSC.

For each PSC, a displacement over time graph is created and the displacement of mm/year is calculated from a linear fit of the points according to Figure 3.2. The displacement values are saved in a matrix which is geo-referenced into a geotiff so that it can be projected on a map. The root mean squared error (RMSE) is calculated for each pixel to see how well the linear fit matches the data and thus give an idea of how the points vary around the linear fit.

The RMSE is calculated as

$$RMSE = \sqrt{\frac{\sum_{i=1}^N (\theta_i - \hat{\theta}_i)^2}{N}} \quad (3.2)$$

where N is the number of images, θ is the data points, and $\hat{\theta}$ is the values of the linear fit evaluated in the data points. A small RMSE indicates a good fit and a large RMSE indicates a large variation around the fit.

3.4 Processing by SkyGeo

Since SkyGeo offers InSAR processing as a commercial product, the exact processing procedure is unknown. However, the processing is based on a phd-thesis [27] written by one of their employees. All information in this section is based on [27].

All images are coregistered to a single master image which is selected carefully since it will affect the results highly. The master is selected so that the coherence is maximized for the entire time series and the atmospheric delay is minimized. This is because the errors associated with low coherence and large atmospheric effects will affect all interferograms if they are present in the master image, and therefore the errors should be as small as possible in the master image.

The PSC selection differs from the processing in SNAP. It is based on the amplitude dispersion method described in section 2.2.2. The reason for this is a proposed maximum number of PSC while minimizing the risk for accidentally neglecting reliable pixels.

The separation of the phase contributions from noise, deformation, and atmosphere is based on assumptions regarding the correlations. It is assumed that the delay caused by the atmosphere is correlated in space but not in time, unmodeled deformation is correlated in time, and noise is not correlated in neither time nor space.

The unmodeled deformation is separated by a weighted temporal low-pass filter. After the separation of the unmodeled deformation, a spatial low pass-pass filter is used for the separation of atmosphere and noise contributions. By doing so, it is possible to remove many of the error sources in the interferogram.

3.5 Result analysis

The output from both SNAP and the SkyGeo processing is essentially images with color-pixels corresponding to the estimated displacement rates. The PSI result only shows the result for the PSC while the DInSAR map shows all the pixels in the image. To analyze the images it must be considered, are the results reasonable? Is the geo-correction good or is there an offset? What are the corresponding coherence values of the pixels?

The accuracy of the geo-correction is important, because if there is an error the wrong pixels is read and a pixel situated off the railway may be interpreted as the railway which can have negative consequences. Railway displacement may be missed because the pixel off the railway showed no displacement. One way to determine if there is an offset is to place a reflector in the area of interest and use a new Sentinel-1 image from when that reflector is present. The location of the reflector should be carefully measured, for example by using GPS measurements. The reflector is easy to detect in the image because of the strong backscatter from it. The location from the GPS and the SAR measurements can be compared and an offset can be calculated and be accounted for. One issue with this solution is that all the images used in this project are already taken and no reflector was placed at the time of the data acquisition.

Another solution is to use the intensity image which is part of the data. In the intensity image, it is possible to see structures like roads, buildings, and railway. Since the pixels for intensity corresponds to the pixels for phase measurements it can be shown that the phase information comes from the railway. A drawback is that the intensity image has a bit low resolution so it is not obvious that it is the railway. Some knowledge that it is expected to find a railway there is required to conclude that it really is the railway. Another way is to use the GeoTiff or Kmz intensity file to plot the intensity in Google Earth or another map. For example, Google Earth has mapped out where the railway is and this can be compared with the supposed railway in the intensity image. A problem with this is that Google Earth or similar map services also have errors in the map projection but if the two coincide, then possible errors can be assumed to be small. This is the option used in this project since it is a simple and yet effective way of projecting the results and see if they correspond.

The coherence consideration is done by looking at the coherence value for the different pixels. In the PSI case, it is known that all pixels have a coherence value above a certain threshold value used for the PSC, because pixels with lower coherence have been sorted out. Before the sorting process of the SNAP processing, the coherence

maps from each interferogram is observed for all interferograms. This gives an idea of which pixels are reliable. A plot is made for the coherence over time in order to see how the coherence value differs over time. This is just done for the SNAP processing because the results from SkyGeo are the output of the processing. Coherence values for the pixels can be read but not how the coherence has changed over time.

In the 2-pass and 3-pass DInSAR case, it is more important to consider the coherence map because all pixels regardless of coherence value are shown. The analysis is made by simply looking at the coherence map and the displacement map and neglect pixels in the displacement map that shows too low coherence.

Whether or not the results are reasonable must be analyzed using previous knowledge. For example displacements large enough to be seen with the naked eye should be detectable in the displacement maps. Similarly, areas that appear to have no motion when looking at them in person should not appear as large displacements in the displacement maps. Further, Trafikverket has good knowledge of the area and has also ordered processed PSI data from SkyGeo over the desired area. The data is acquired by the TerraSAR-X satellite which operates in a higher frequency and has higher resolution than Sentinel-1. The TerraSAR-X data is compared with the Sentinel-1 data to see how well they correspond. Different values are expected since the resolution and number of input images differ. The idea is that the data from the two different satellites should highlight the same areas as problem areas and that the values should be at least similar.

The comparison between the Sentinel-1 data processed with SNAP and the TerraSAR-X data processed by SkyGeo does not give a correct representation of the differences between the satellites and cannot be seen as a comparison between the satellites. The reason for this is that the different processing methods and error handling will also affect the results. Therefore, a comparison between the two would rather be a comparison between the processing methods. To solve this issue, SkyGeo has processed Sentinel-1 data and provided the results using the same processing procedure as they used for the TerraSAR-X data and from the same time period as the TerraSAR-X measurements. The TerraSAR-X data processed by SkyGeo and the Sentinel-1 data processed by SkyGeo is compared to find differences between the satellites. Further, the Sentinel-1 data from SkyGeo and the Sentinel-1 data processed in SNAP are compared to see how the error sources affect the data.

An interesting parameter other than the absolute values of the displacement rates is the RMS error of the linear fit. Since the displacement rates are estimated from the linear fit the RMS error gives an idea of how well the actual data follows the linear fit. The RMS error of the 3 different cases: TerraSAR-X by SkyGeo, Sentinel-1 by SkyGeo, and Sentinel-1 in SNAP will be calculated and compared.

3.6 Compare PSI and Optram

Measurement trains that performs measurements that are stored in Optram is the currently used measurement technique at Trafikverket to detect movement or irregularities in the rails. A measurement train drives along the track and makes relative measurements of the position of the rails, thus Optram does not provide absolute measurements of the position. The measurement trains used are called IMV100 and IMV200 and they look like regular trains. IMV100 is just a locomotive and IMV200 is a rebuilt restaurant car. The IMV100 train can measure at 80 km/hour and the IMV200 train can measure at 200 km/hour. However, because of a lack of available locomotives the train is seldom operated at speeds above 160 km/hour. Using these trains, the main tracks in Sweden are measured six times annually [28, 29].

Trafikverket maps the entire railway network in Sweden by referring to different "railway meters" and kilometer numbers along the track to keep track of different parts of the railway. By using relative measurements over a certain length and keeping track of which kilometer number that the measurement took place at, georeferencing is possible but not very accurate. This is not an issue for Trafikverket's maintenance work as the kilometer number is the common terms of reference, but this imposes a problem when comparing the Optram data to InSAR data.

Since the goal is to use both Optram and InSAR and let the measurements complement each other, it is desired to connect the measurements. One system could not replace the other since Optram is measuring the railway and InSAR is mainly measuring the railway embankment. By combining the two, it could be possible to say at an early stage if the railway moves because it is bad or if it is because the ground is moving. It could also give an answer to if only the rails or both rails and embankment moves. To test this, problem areas detected by Optram and problem areas detected by InSAR are compared to see if they can be seen by both measuring techniques.

4

Results

This chapter presents the results from the different measurements and describes shortly what can be seen. A more thorough discussion is given in the discussion chapter. This chapter also presents the acquisition dates of the data.

4.1 Intensity measurements

As mentioned in section 3.5, the intensity measurement is important for finding structures in the image which can be used to see what actually causes the reflection.

A single intensity image is quite noisy and may suffer from pixels that show a strong/weak reflection by chance at that particular time. To avoid such effects, the intensity image is made as the mean value of 10 consecutive intensity measurements from March to June 2018 by the Sentinel-1 B platform. By doing so, the noise is reduced and the strong pixels are more stable because it means that they have given a strong reflection over time. By averaging the magnitude values in the time domain rather than spatial domain, the spatial resolution of the image is preserved. The result can be seen in figure 4.1.

It is clear that figure 4.1 shows a lot of details. Hills, lakes, and buildings can be seen and the bright line going diagonal in the image appears to be the railway. As stated previously, it is likely the railway but without prior knowledge that a railway is expected in that area, it is difficult to confirm that it is the railway. The intensity image projected in Google Earth is shown in figure 4.2.

In the map projection, it is obvious that the bright line across the image coincides with the railway according to Google Earth. While both the Google Earth map and the intensity image have uncertainties and errors in their respective geo-referencing process, they coincide to a large extent meaning that it can be concluded that it is the railway and that the geo-referencing of the Sentinel-1 data works well.



Figure 4.1: Intensity averaged from 10 intensity measurements between March and June 2018. The Figure contains modified Copernicus Sentinel-1 data [2019].

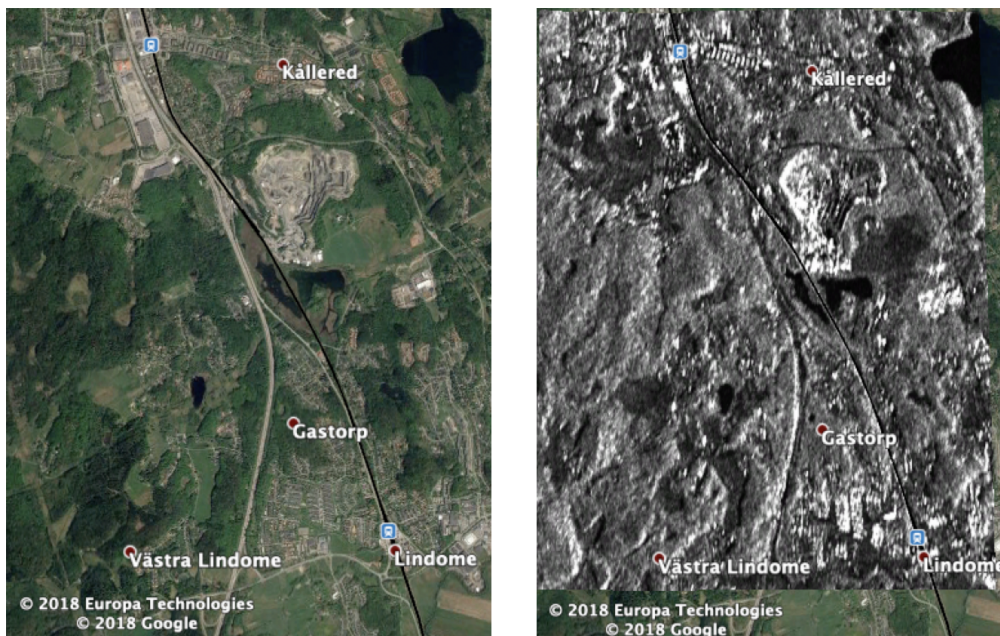


Figure 4.2: Google Earth image over the area (Left) and the intensity image map projected in Google Earth (Right). The Google Earth image shows the train stations and railway (contains modified Copernicus Sentinel-1 data 2019).

4.2 DInSAR in SNAP

The 2-pass DInSAR measurement uses data from the 9 July 2018 (master) and 27 July 2018 (slave), which means a temporal baseline of 18 days. The 3-pass DInSAR measurement uses the same acquisitions but the DEM is created between the acquisition on 9 July (master) and an acquisition on 3 July (slave). The displacement maps are cropped for Lindome and Kållerød station respectively so that the displacement around the stations can be seen more clearly.

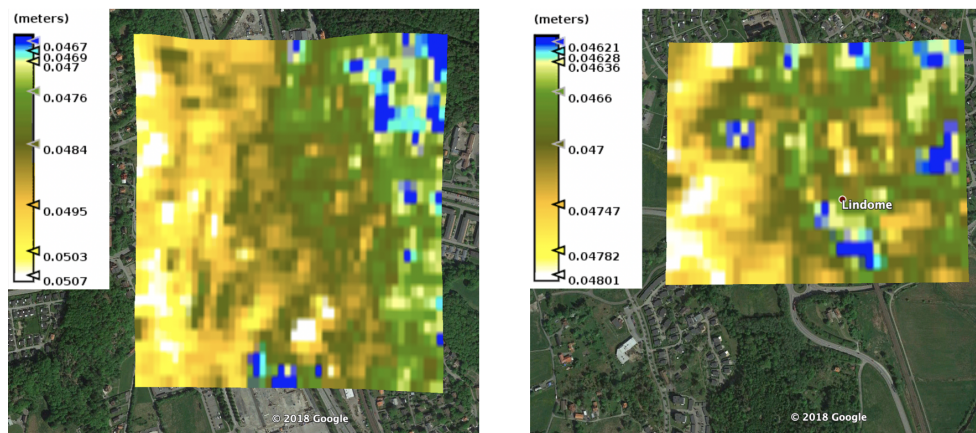


Figure 4.3: Displacement maps of Kållerød station (Left) and Lindome station (Right) obtained by 2-pass DInSAR with Sentinel-1 data and the SRTM DEM with a temporal baseline of 18 days. The displacement maps are projected in Google Earth.

Figure 4.3 reveal some issues with the 2-pass differential technique. For example, the scale shows that there are only positive values present. This implies that there is only uplift and no settlement in the area which is highly unlikely. Because of the known settlement issues in the area, some pixels that indicate settlements in the images are expected.

Another issue is the absolute values of the results. The colorbar indicates an uplift of 4-5 , which is extremely large considering the short time period of 18 days. Values of that magnitude are not expected and especially not over such large areas. To give some perspective, a displacement rate of over 5 cm a year is considered problematic so a displacement rate of 4-5 cm in 18 days is not reasonable, especially not for all of the area.

The large displacement rates are possibly results of the neglected phase contributions in eq. (3.1). Since the terms were not removed, they are misinterpreted as displacement which increases the uncertainty of the displacement values. Also, phase unwrapping is a difficult process that can be disturbed by noise or changes on the surface, for example transitions between land and water. Although a filter is used to remove the noise, some residuals may be enough to disturb the unwrapping

4. Results

algorithm causing the entire area to be mapped in the wrong phase cycle. This may be an explanation for the strictly positive values.

The corresponding coherence values from figure 4.3 can be found in figure 4.4.

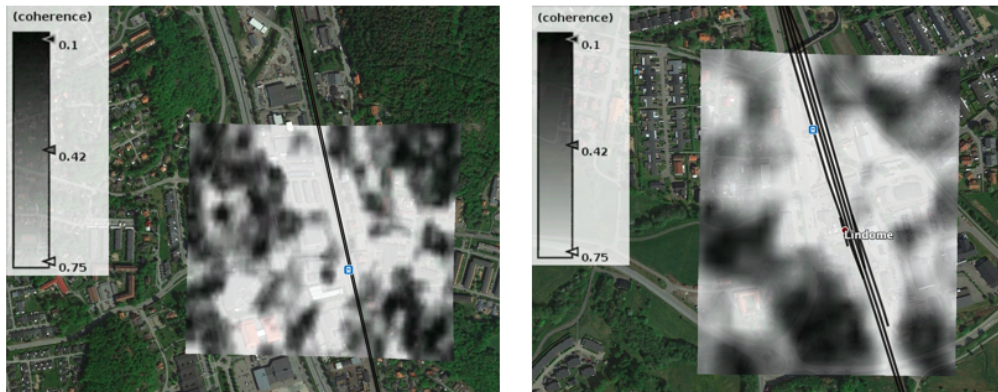


Figure 4.4: Coherence values corresponding to the 2-pass DInSAR images of Källered station (Left) and Lindome station (Right). The coherence values are map projected in Google Earth. The Figure contains modified Copernicus Sentinel-1 data [2019].

Figure 4.4 shows quite high coherence over both areas and especially for the railway. This implies that the unreasonable displacement rates do not depend on a lack of reliable scatterers.

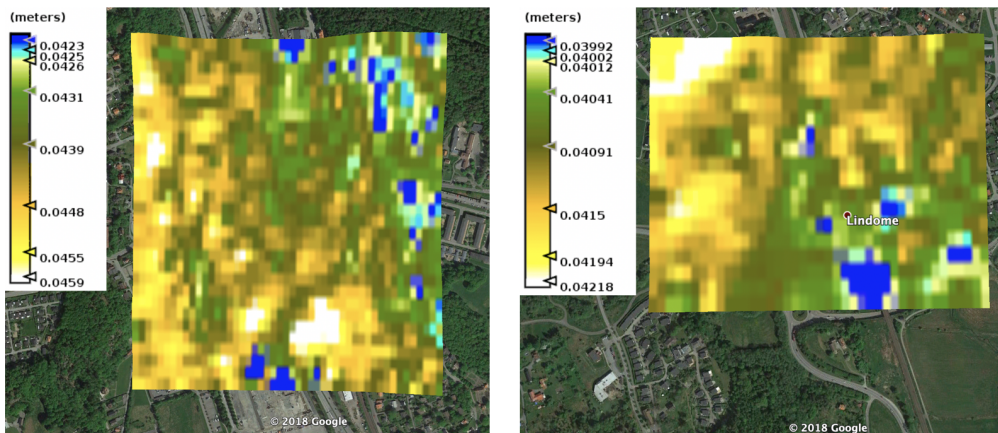


Figure 4.5: Displacement maps of Källered station (Left) and Lindome station (Right) obtained by 3-pass DInSAR using Sentinel-1 data.

Also in the 3-pass case, Lindome station shows exclusively pixels with uplift with large magnitudes. These are like in the 2-pass case possibly caused by neglecting some phase contributions that become misinterpreted as displacement. Mistakes in the unwrapping algorithm are also probable.

Coherence maps related to the displacement maps in figure 4.5 are shown in figure 4.6.

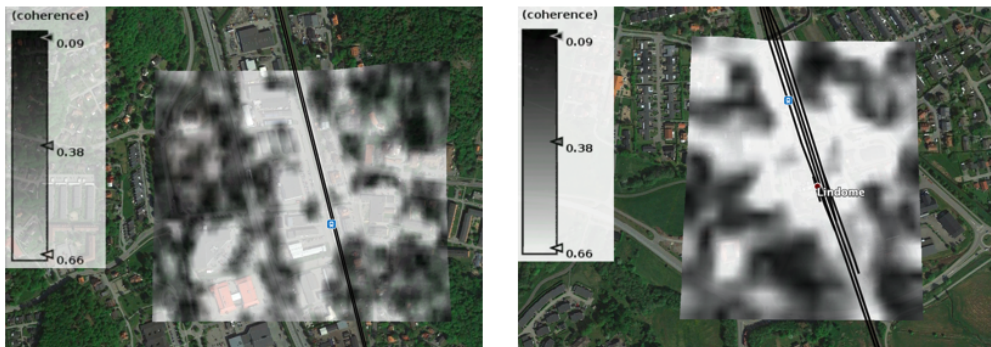


Figure 4.6: Coherence values corresponding to the 3-pass DInSAR images of Källered station (Left) and Lindome station (Right). The coherence maps are map projected in Google Earth.

4.3 PSI with TerraSAR-X

The data stack consists of 79 images acquired between 2 January 2016 and 7 September 2018. All the images are acquired from descending mode of the satellite. The displacement is calculated in the vertical direction under the assumption that there is no horizontal movement by using the incidence angle. Displacement maps for Källered and Lindome station are shown in Figure 4.7 and for the entire area of interest is shown in Figure 4.8. All the TerraSAR-X data were processed by SkyGeo and provided as a finished product to WSP and Trafikverket. The data are used with permission from SkyGeo, WSP, and Trafikverket.

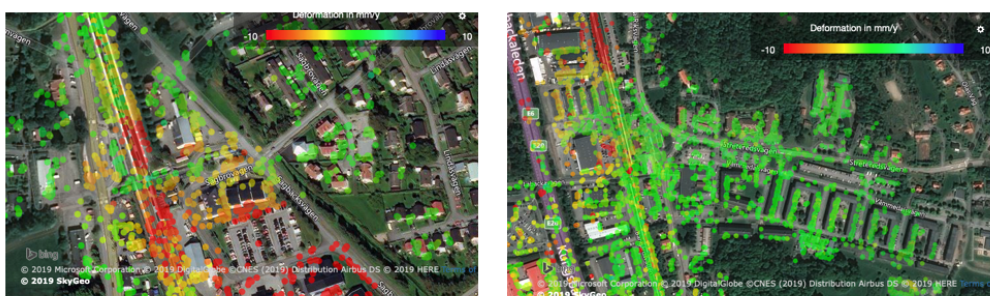


Figure 4.7: Displacement maps over Lindome station (Left) and Källered station (Right) using TerraSAR-X data. Note that the dots do not represent the pixel size, they show the center of the pixel. The images are courtesy of SkyGeo and used with permission from SkyGeo, WSP and Trafikverket. The data are shown in a map by Bing.

Because the results from the TerraSAR-X measurements have been analyzed by Trafikverket and have been compared to on-sight observations by Trafikverket, the

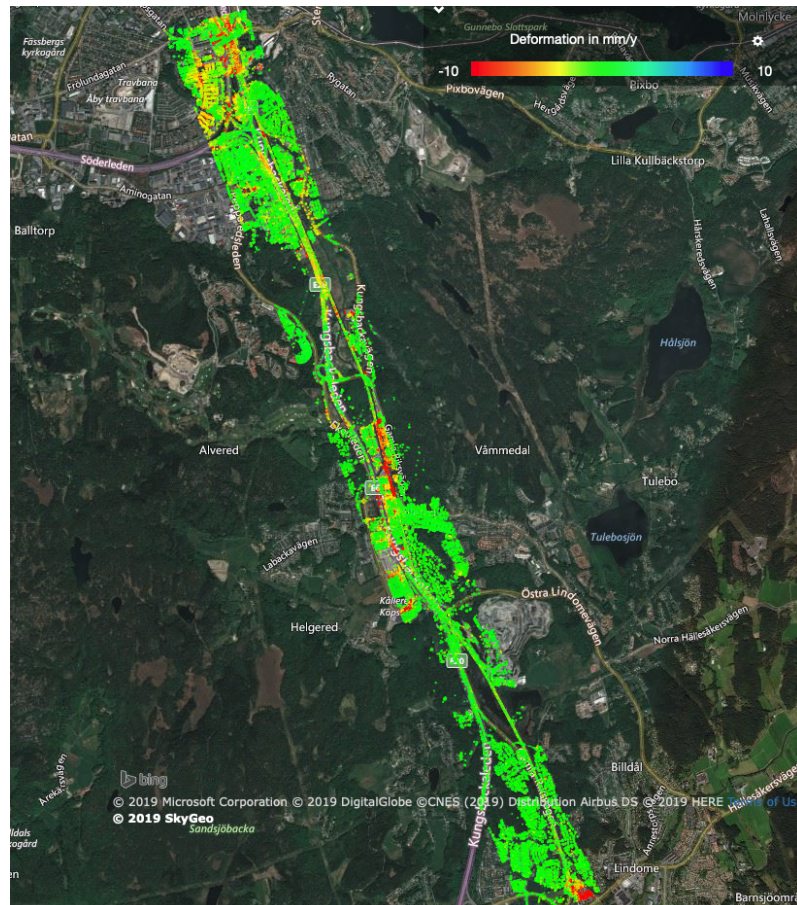


Figure 4.8: Displacement map over the total area of interest analyzed from TerraSAR-X data. The processing is done by SkyGeo. The image is courtesy of SkyGeo and used with permission from SkyGeo, WSP and Trafikverket. The data is shown in a map by Bing.

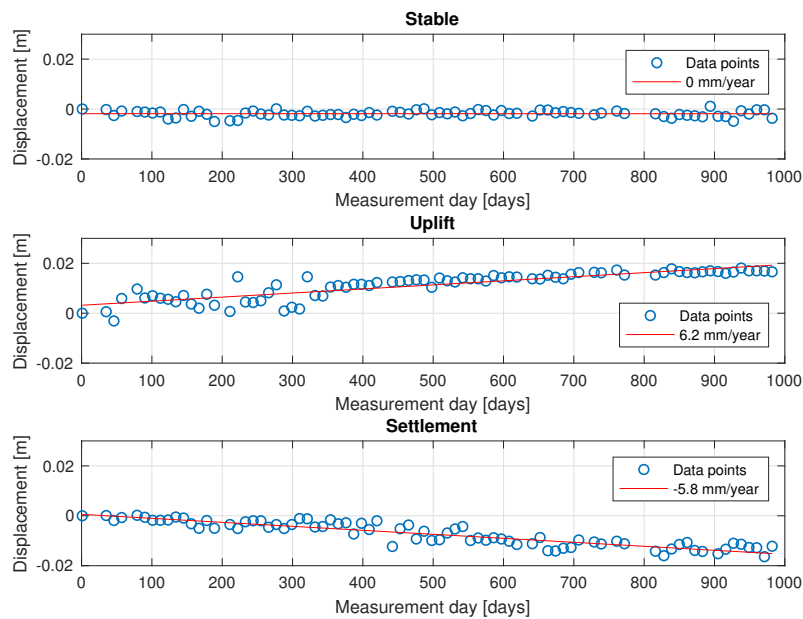


Figure 4.9: Displacement over time for the TerraSAR-X data for a stable point (Top), uplift (Middle), and settlement (Bottom).

data are regarded as reference. The absolute values have not been verified, but the areas that show problematic settlements match the known problem areas. For example, the left image of Figure 4.7 is showing a red area with a green line going across it. The green area is a tunnel for pedestrians under the railway tracks. This tunnel is stable, but the area around it is sinking and almost wrapping around the tunnel. This is a problem known to Trafikverket and can be noticed with on-site observations. See Figure 4.10. It is desired that Sentinel-1 shows similar results.

It can be observed that there are results from many pixels over the area. Displacement plots from some of them are shown in Figure 4.9.

It can be seen that regardless of the movement of the pixel, the measurements follow the linear fit well. Although there are some fluctuations of the results, the pixel with uplift shows a clear uplift, and opposite for pixels that show settlements. This is also observed when looking at the RMS error which is calculated for all the pixels in the area of interest. The RMS error is then somewhere between 0.5 and 3.9 mm. The distribution of the RMS errors are shown in a histogram in Figure 4.11. It can be seen that most of the RME error values are around the mean value with a slightly larger peak around 2.5 mm.

The RMS errors do not seem to be affected by the area. For example by buildings, railway, roads, or vegetated areas. However, it appears to be a connection between a high coherence value of a pixel and a low RMS error. Note that the coherence value denotes the stability of the pixels in the interferograms and that the RMS error is the variation between the linear fit and the data points. Large variations in displacement are not necessarily caused by phase instabilities.



Figure 4.10: Photo of the railway track at Lindome station. It is possible to see how the railway tracks and platform form a slope after the tunnel.

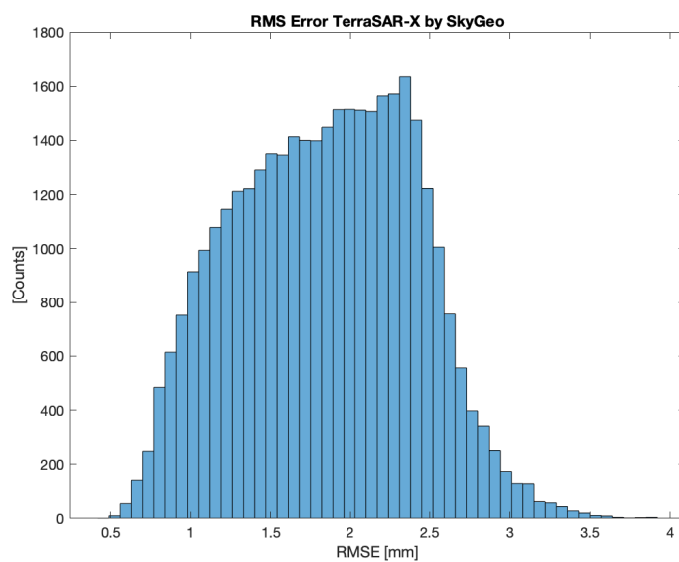


Figure 4.11: Histogram of the RMS errors in the results from TerraSAR-X.

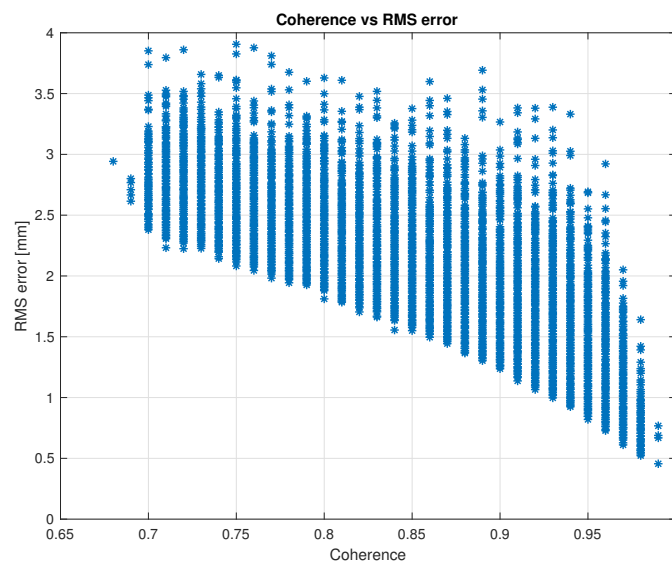


Figure 4.12: RMS errors plotted as a function of the coherence of the TerraSAR-X results by SkyGeo.

To test the coherence and low RMS error hypothesis, the RMS errors are plotted as a function of the coherence. The result can be seen in Figure 4.12. The reason for why the points appear in vertical lines in the graph is that the coherence values are rounded to two decimal points. The rounding of the values causes some of the coherence values to show higher RMS errors than they should since if more decimal points were included, it is probable that some points would move to the left or right in the figure and not appear as straight lines. It still possible to see a trend that the RMS errors are lower for higher coherence values which supports the hypothesis.

4.4 PSI in SNAP

The data stack consisted originally of 30 images acquired between 5 March 2018 to 29 April 2019. The data from 2019 lies outside of the time span of the TerraSAR-X and Sentinel-1 by SkyGeo stacks and is therefore removed from the stack. It was originally included to see how measurements with larger time spans affected the results, and data before 2018 was at the time unavailable from the Copernicus Hub. The images from 5 March, 15 March, and 29 March are excluded because they showed low coherence possibly caused by weather conditions during the early spring. The decision to exclude them is partly made after reading [24], who only include acquisitions from June to October each year because of the weather conditions. Because the April data gave acceptable coherence, these images were included. After the removal of the acquisitions in March and outlier data, the final stack for the PSI analysis thus consists of 21 images between 10 April 2018 and 31 October 2018. In total, two acquisitions are removed because they appear to be outliers. All of the images are acquired from descending orbit and the displacement values are converted

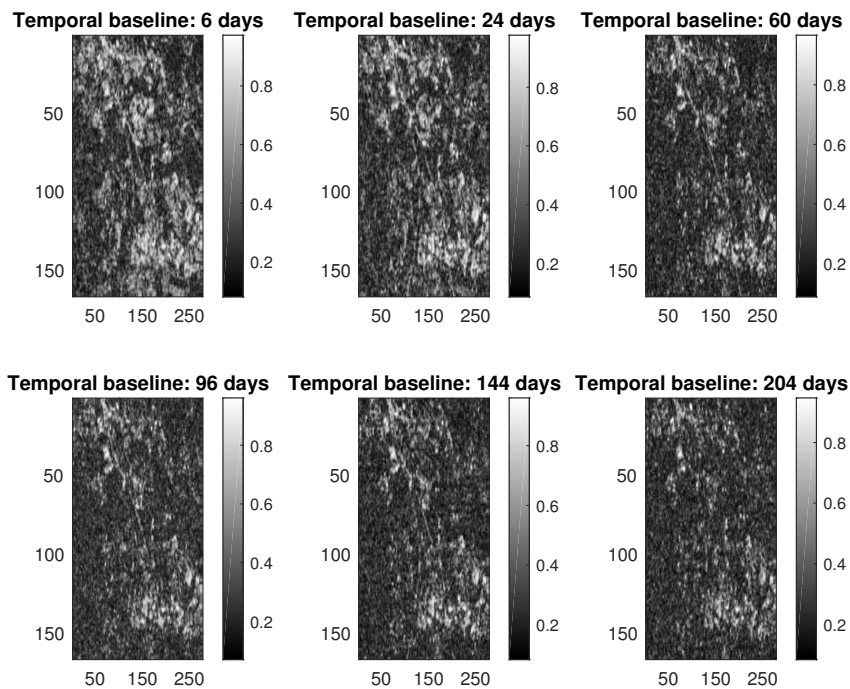


Figure 4.13: Coherence maps over time for the area of interest for the Sentinel-1 data.

to vertical direction using the incidence angle under the assumption that there is no horizontal displacement.

Before the the PSC selection, the coherence must be known. A coherence plot for 6 of the baselines with different temporal baselines are shown in Figure 4.13. With some previous knowledge from looking at the intensity images, it can be seen that the railway appears as a bright line through the middle of the coherence images as well. This indicates that the railway shows high coherence while areas other than the urban areas decorrelate over time. However, one can observe that the railway becomes fainter over time and is not clearly visible in the coherence plot with a temporal baseline of 204 days. The coherence does not drop completely but becomes lower than expected.

Coherence plots over time for some selected pixels are shown in Figure 4.14. The good and bad points are selected as typical points that have high and low coherence respectively over the time span. The railway pixel is selected as a typical railway pixel, that is most railway pixels show similar behaviour.

It is observed that the railway decorrelates over time and that the railway pixels are not the most stable points in the image. However, coherence is not the only way to estimate phase stability. As mentioned earlier, a strong intensity can also be an indication of phase stability. From Figure 4.1, it is clear that the railway gives a relatively strong backscattered intensity so that the assumption is made that the railway pixels are allowed to show a lower coherence down to 0.3 and still be

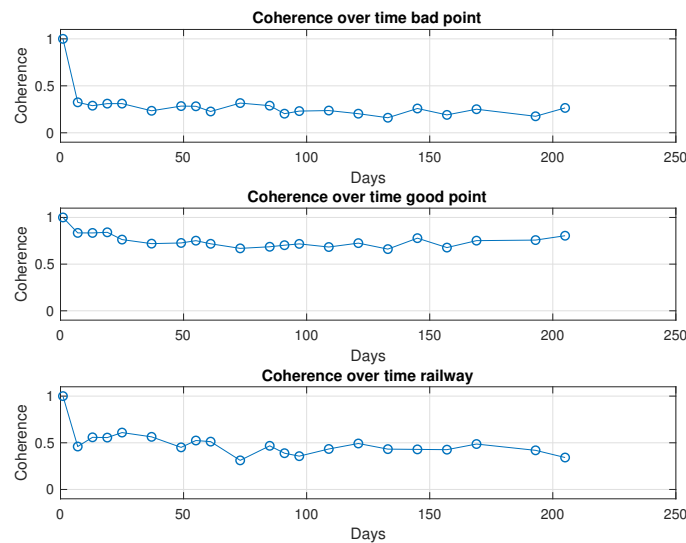


Figure 4.14: Coherence plotted for 3 different pixels in the Sentinel-1 data processed in SNAP. Top) A typical bad pixel Middle) A typical good pixel Bottom) A typical railway pixel.

assumed to have a stable phase. Thus, the PSC are all the pixels with a coherence larger than 0.3.

The displacement maps for Lindome and Kållerød are shown in Figure 4.15. The colors fill the entire pixel so that the maps show the actual pixel size. It can be seen that the Lindome map shows moderate settlements and uplift and that the Kållerød map shows mainly strong uplift. This is not expected when looking at the TerraSAR-X results. A possible cause is that the different processing methods and different error handling causes different amounts of error residuals in the result that are included in the displacement maps. At least, the differences cannot be concluded to come entirely from the differences of the satellites, but also from the difference in processing.

To see how the data is varying around the linear fit, the data from selected points are shown in Figure 4.16. The points are taken from different locations in the image and they are not located closely together. It is clear that although the estimated displacement rate is quite different, the data points look similar in the three graphs, and this is the case for all the pixels in the image. This can possibly be explained by errors that affect the entire image and not just on local scales since all pixels show similar results in most cases.

It is just small variations and a difference in a few points that make up the difference of whether the point shows $+20$ mm/year or -10 mm/year. The fact that so few points can change the displacement rate so drastically can partly be explained by a short time series but the large variations is also an issue for the measurements. It means that the displacement rate estimation is unreliable and similarities to the other data may just be coincidences. The data series show both uplifts and settle-

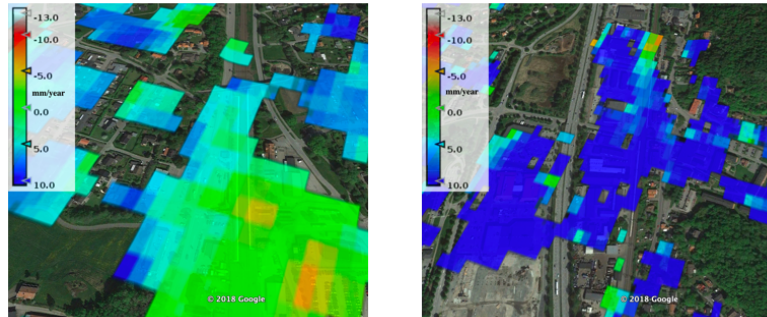


Figure 4.15: Displacement maps for Lindome station (Left) and Källered station (Right) using the Sentinel-1 data processed in SNAP. The map projections are done in Google Earth.

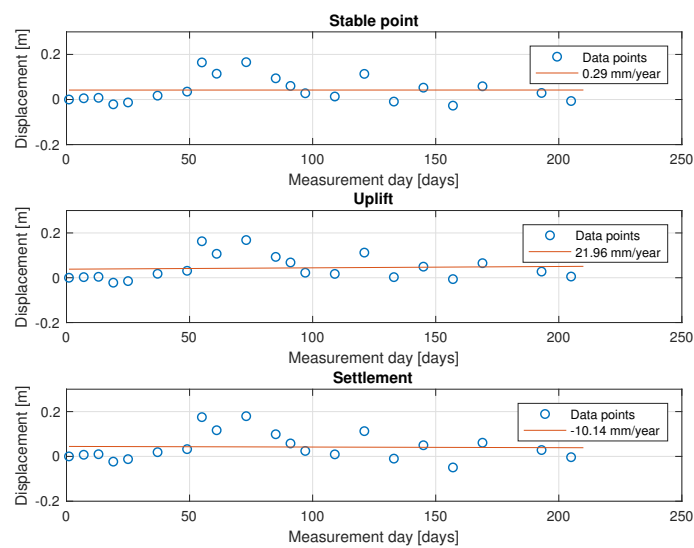


Figure 4.16: Displacement over time for a stable point (Top), point with uplift (Middle), and point with settlement (Bottom) from the Sentinel-1 data processed in SNAP.

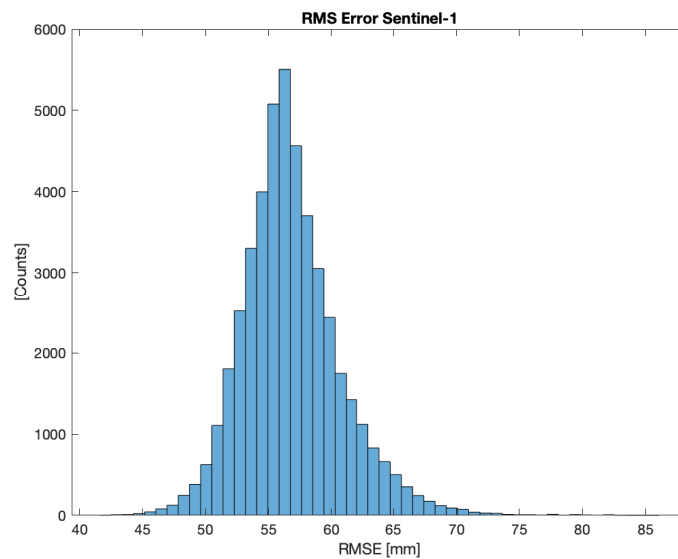


Figure 4.17: Histogram of the RMS error of the results from the SNAP processing of the Sentinel-1 data.

ments and the net result can be either depending on just a few images.

The RMS errors for the displacement estimations lie between 41.7 and 86.0 mm which further proves that the displacement values are unreliable. A histogram of how the errors are distributed is shown in Figure 4.17. Most of the values are around the mean RMS error.

Because of the low coherence values and large RMS errors of the data, no cross-correlation is done. It is difficult to find a connection for the RMS errors and it is also considered unnecessary since all the RMS errors are so large for the data so that it is considered unreliable.

4.5 PSI with Sentinel-1 by SkyGeo

The data stack consists of 143 images acquired between 1 June 2016 and 17 May 2019. All images are acquired from descending orbit and the displacement is converted to vertical direction by using the incidence angle under the assumption that there is no horizontal displacement. The results from the Sentinel-1 data was processed by SkyGeo using the same processing procedure as they did with the TerraSAR-X data. The results are courtesy of SkyGeo and used with permission from SkyGeo.

Because the same processing was used by SkyGeo with the Sentinel-1 and TerraSAR-X data, by comparing the two it should be possible to compare the different satellites. However, different acquisition dates and different number of acquisition dates still affect the result, but the processing should not affect it.

4. Results

Displacement maps of Källered and Lindome stations are shown in Figure 4.18 and of the total area of interest is shown in Figure 4.19. Graphs showing the displacement of some pixels are shown in Figure 4.20. It can be noted that although some variations around the linear model is present in the data, the points still follow the trend. There is no ambiguity whether the point is approximately stable, settles or lifts.



Figure 4.18: Displacement maps over Lindome station (Left) and Källered station (Right) using Sentinel-1 data processed by SkyGeo. Note that the dots do not represent the pixel size, they show the center of the pixel. The images are courtesy of SkyGeo and used with permission from SkyGeo, WSP and Trafikverket. The data is shown in a map by Bing.

The RMS errors for the displacement of the pixels are calculated to lie between 1.3 and 9.7 mm which is larger than for the TerraSAR-X results but smaller than for the analysis in SNAP. The distribution of the RMS errors are shown in a histogram in Figure 4.21. Some of the larger peaks are tilted to the right of the mean value which means that a larger RMS error is more common in the measurements, but the width of the histogram shows that the RMS errors are still spread out.

The RMS errors are plotted as a function of the coherence to see if there is a correlation. The result is shown in Figure 4.22. These coherence values are not rounded to two decimal values like in the TerraSAR-X case and thus the curve gets a different shape. It can be seen clearly that the RMS errors decrease for increasing coherence, thus also in the Sentinel-1 result from SkyGeo it can be expected to find small RMS errors where there is high coherence.

Since all the data stack for Sentinel-1 results by SkyGeo, and Sentinel-1 results from SNAP have a different number of acquisitions, a comparison between them would not be completely accurate. More data points implies statistically reduced errors and differences in the results may be a result of that. Therefore, the Sentinel-1 results from SkyGeo are reduced to match the other result. Since both stacks come from Sentinel-1, the exact same acquisitions have to some extent been used in both data stacks. There are only 2 acquisitions in the stack used for the processing in SNAP that are not present in the stack used by SkyGeo. Those are changed to acquisitions close in time so that the number of acquisitions match. Figure 4.20 is recreated with the same pixels but using just the acquisitions from the stack used in SNAP. The result is shown in Figure 4.23. Except for the 2 acquisitions that do not match in the data sets, the differences in the results from SkyGeo and

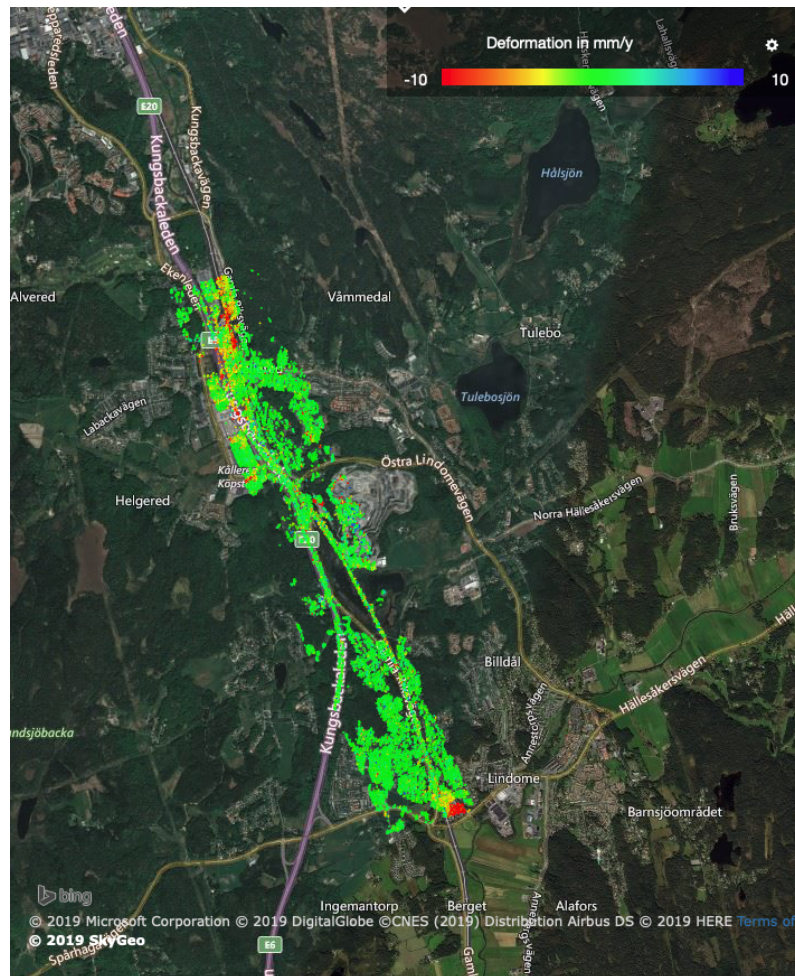


Figure 4.19: Displacement map over the total area of interest from Sentinel-1 data. The processing is done by SkyGeo. The image is courtesy of SkyGeo and used with permission from SkyGeo, WSP and Trafikverket. The data is shown in a map by Bing.

4. Results

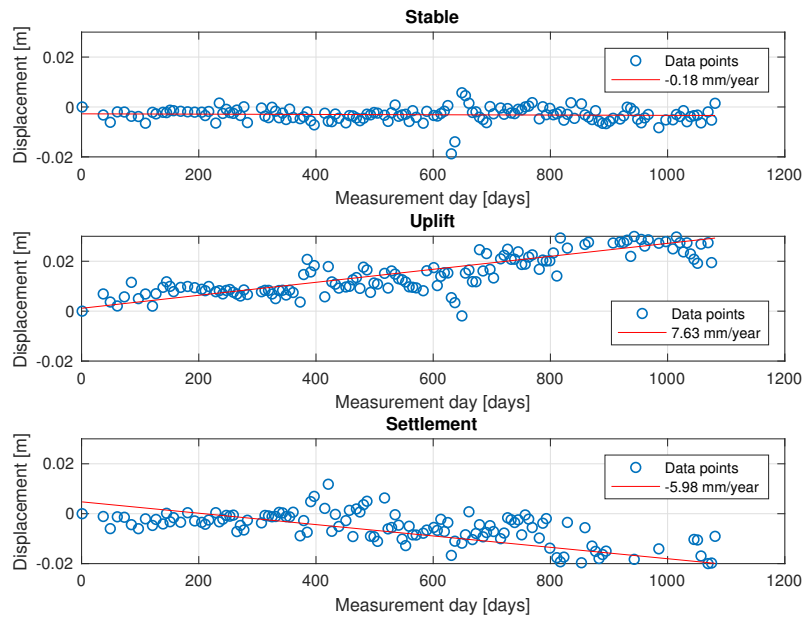


Figure 4.20: Displacement over time for a stable point (Top), point with uplift (Middle), and point with settlement (Bottom) from the Sentinel-1 data processed by SkyGeo.

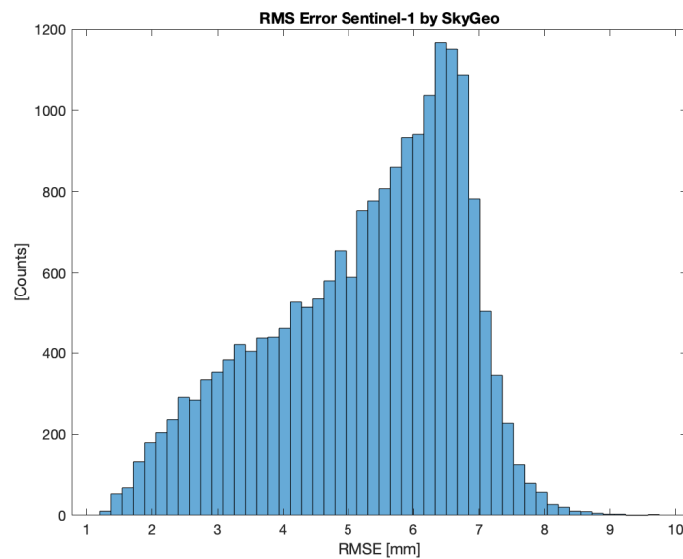


Figure 4.21: Histogram of the RMS errors from the Sentinel-1 results analyzed by SkyGeo.

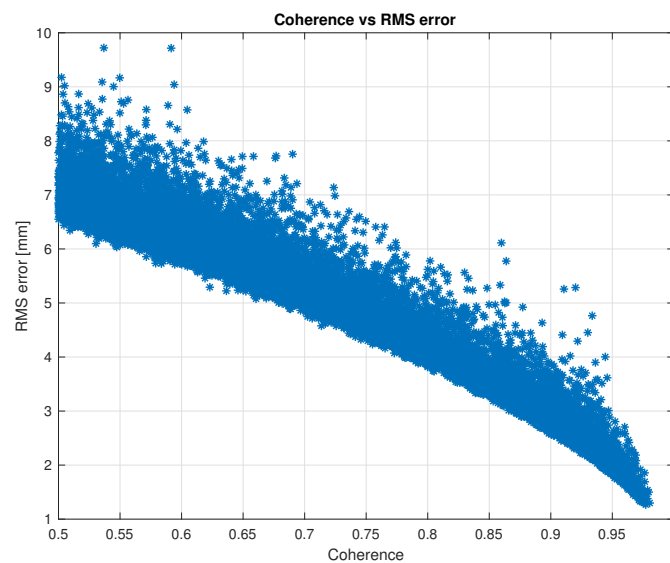


Figure 4.22: RMS errors as a function of coherence of the Sentinel-1 results processed by SkyGeo.

the SNAP results should only be caused by the different processing methods. The results show less ambiguity than the results from the SNAP processing. Just like for the entire Sentinel-1 stack by SkyGeo, it is clear that a point with uplift shows uplift and that a settling point is showing a clear settlement. The old displacement rates of -0.18 , 7.63 , -5.98 mm/year has become -1.65 , 23.01 , and -22.17 mm/year for the same points. The RMS errors of this shorter stack lie between 0.5 and 12.7 mm which means that there are points with smaller RMS errors in this short time period compared to the entire stack by SkyGeo, but there are also larger RMS errors. The larger RMS errors are expected because there are less data points. The distribution of the RMS errors are shown in Figure 4.24. Because no comparison is made between RMS errors and coherence for the SNAP results, that is not done for the shorter Sentinel-1 by SkyGeo stack either.

Finding similarities in the acquisition dates of the TerraSAR and Sentinel data is more difficult. The TerraSAR data is acquired from 2016-2018 and Sentinel data is missing for the first five months of 2016 but the Sentinel stack contains approximately five months of data in 2019. Also the Sentinel-1 satellites have a shorter time period between acquisitions than TerraSAR-X. However, this should be considered a positive feature of Sentinel-1 in the same way as higher spatial resolution is a positive feature of TerraSAR-X. Therefore, all the Sentinel data within the time period should be included as the shorter temporal baselines should be a part of the comparison. Because the Sentinel data lacks five months of data in 2016 but has approximately five months of data in 2019 which is not used in the TerraSAR-X result, the results of the entire stacks of Sentinel and TerraSAR-X data are used. This means that the result is based on roughly three years of TerraSAR-X and three years of Sentinel-1 data, but the Sentinel-1 data is shifted five months. This shift should be considered in the analysis but is accepted in order to have an equal time

4. Results

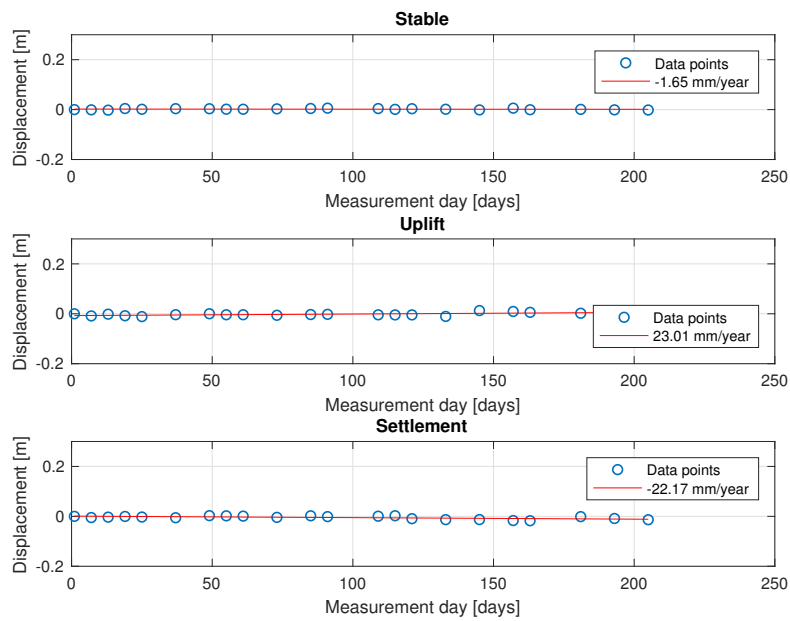


Figure 4.23: Displacement over time for the same points as in Figure 4.20 but using a shorter stack.

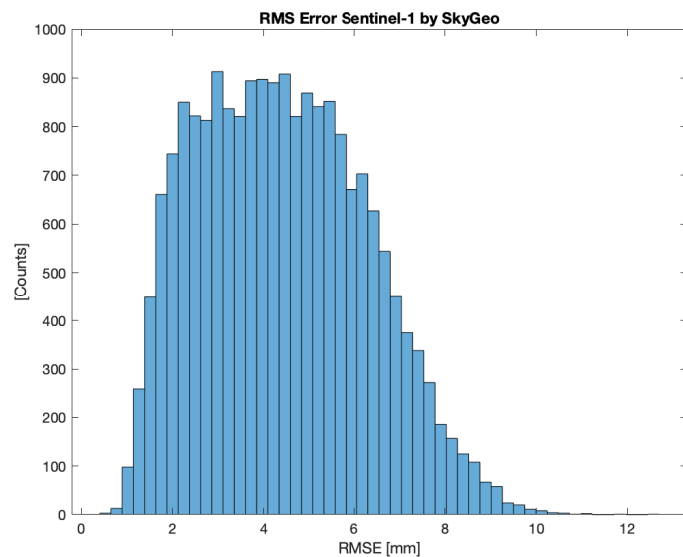


Figure 4.24: Histogram of the RMS errors from the Sentinel-1 results analyzed by SkyGeo with fewer acquisitions used.

period between the satellites, see Section 5.3.

To compare the displacement rates acquired from TerraSAR-X by SkyGeo, Sentinel-1 by SkyGeo and Sentinel-1 in SNAP respectively, the displacement rates along the railway track in Källered and Lindome are analyzed. The displacement rates along the track are plotted with respect to a position on the track. The result can be seen in Figures 4.25 and 4.26. The x-axis denotes the relative position of the measurement point on the track but the x-axis should be considered unitless. Note that since all three acquisition methods have found different PSC, there is a slight offset in x-direction and a different number of points for the different methods. The aim of the comparison is to give an idea of how the trends coincide with each other. As previously stated, when comparing the Sentinel-1 data from SkyGeo and in SNAP, the time period should be the same in order to make a more qualitative comparison. However, in this case, it is desired to make a comparison for the best possible scenario for all three methods and thus the results from the entire available stacks are used. Comparing the methods using different time periods could impose a problem that is discussed further in Section 5.2.

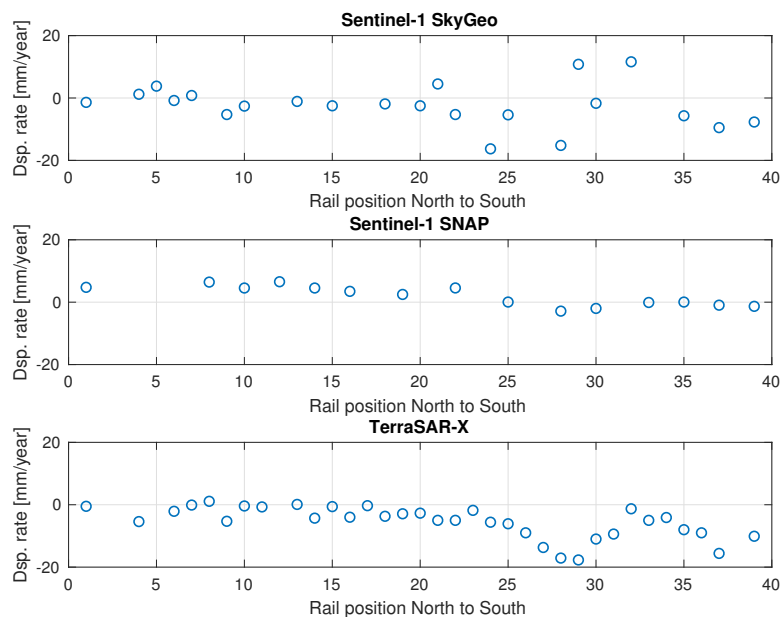


Figure 4.25: Displacement rates along the tracks at Lindome station from Sentinel-1 by SkyGeo (Top), Sentinel-1 in SNAP (Middle) and TerraSAR-X by SkyGeo (Bottom). The first point is approximately 100 m north of the platform and continues to approximately 100 m south of the platform. The time periods are June 2016 - May 2019 for Sentinel by SkyGeo, January 2016 - September 2018 for TerraSAR-X by SkyGeo and April 2018 - October 2018 for Sentinel in SNAP.

It can be seen in Figure 4.25 that Sentinel-1 by SkyGeo and TerraSAR-X coincide roughly, and that the tunnel can be seen around the value 30 on the x-axis. The difference is that Sentinel-1 by SkyGeo shows uplift where the TerraSAR-X results

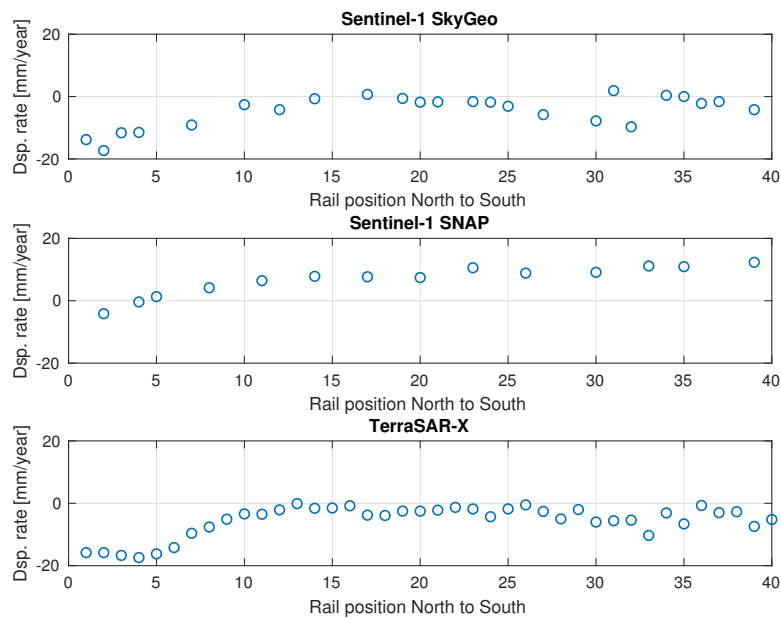


Figure 4.26: Displacement rates along the tracks at Källered station from Sentinel-1 by SkyGeo (Top), Sentinel-1 in SNAP (Middle) and TerraSAR-X by SkyGeo (Bottom). The first point is approximately 100 m north of the platform and continues to approximately 100 m south of the platform. The time periods are June 2016 -May 2019 for Sentinel by SkyGeo, January 2016 - September 2018 for TerraSAR-X by SkyGeo and April 2018 - October 2018 for Sentinel in SNAP.

shows stable ground. This uplift is only seen in descending orbit and not in ascending and those points may thus be explained by horizontal movement that is wrongly interpreted as vertical movement. Further, it can be observed that the curve from the SNAP results have a similar shape but is shifted upwards. It maintains roughly the same value while the other methods show stability and decreases where the other methods do as well to indicate the displacement around the tunnel. If the SNAP results are shifted downwards so the first stable points appear around zero, the curves look quite similar with the exception that the tunnel would still not appear as clearly as it does in the TerraSAR-X results.

Also in Figure 4.26 it is clear that Sentinel-1 by SkyGeo and the TerraSAR-X results show similar trends. However, here it is even more clear than in Figure 4.25 that the SNAP results show the same trend as the others but shifted upwards in the graph. If the graph was shifted down it would look very similar to the other results. Thus, although the displacement maps in Figure 4.15 appeared to be wrong compared to the displacement maps in Figures 4.7 and 4.18 the error depends on a shift towards uplift in the SNAP data. Possible explanations of the shift are discussed in Section 5.2. Another feature that can be noted is that although Sentinel-1 and TerraSAR-X by SkyGeo show similar trends, the values of the different points do not coincide perfectly. Therefore, the measurements should be used to highlight trends and not to measure absolute values of the displacement rates.

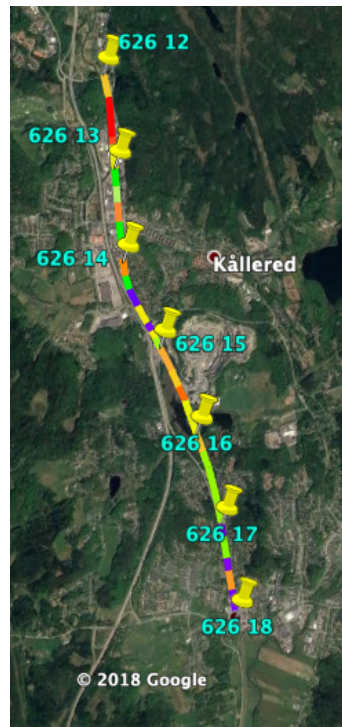


Figure 4.27: Results from Optram plotted in Google Earth. The pins have accurate positions of the track kilometers (turquoise numbers) but the colors inbetween are not perfectly scaled. The data is used by permission from Trafikverket.

4.6 Optram

Trafikverket has provided results from Optram where data from the currently used measurement technique is stored. The result is shown in Figure 4.27. The pins in the image denotes the track kilometers which is the standard railway positioning unit used by Trafikverket. The pins are placed on the map with coordinates of high accuracy provided by Trafikverket. The colors inbetween are not perfectly scaled. The measurement comes from the North-going track and measures standard deviation of the height of the rails. Green denotes small variations (stable) and red-purple denotes large variations (settlement/uplift). Yellow and orange indicate medium sized variations.

5

Discussion

In this chapter, the results are discussed before a final conclusion is made in the conclusion chapter.

5.1 DInSAR in SNAP

Processing InSAR images proved to have a difficult startup period. Although SNAP has a user friendly interface and includes a lot of useful functions and algorithms, some theoretical knowledge of InSAR processing is required. Functions exist for the different processing steps but the order of the different processing steps and the processing parameters for each function must be selected by the user. Many input parameters like for example whether or not to remove the topographic phase in the interferogram formation makes a large difference and therefore requires the user to know the implication of the decision. Things like these makes InSAR processing difficult at first.

After gaining some understanding of the steps of InSAR processing, SNAP appeared to be quite user friendly and easy to use. Many different types of results can be obtained, displacement, height, elevation, to name some of the possible InSAR outputs. Also regular SAR and optical images can be processed. Because the software is written for Sentinel, it is easy to work with the data in the software.

From the results it is clear that the errors and uncertainties are too large as the magnitude of the values are not reasonable. These can be explained by neglected phase contributions other than topography and displacement or possibly that the phase unwrapping procedure added some errors. The amount of noise and other error sources could be minimized by building up a stack of images, but stacking is not fully possible in SNAP at the moment. However, it is possible to extract the data and to write an algorithm in another program. In order to thoroughly test 2-pass and 3-pass in SNAP, a larger effort should be put into processing the same images and do a parameter sweep on the processing parameters to test more thoroughly how different values affect the results. Because of the vast number of possible values to test, such an experiment would take a lot of time. Since DInSAR in SNAP is just one of the parts of this project and because 2-pass and 3-pass interferometry naturally neglects some error sources and does not use a stack of image, there are limitations in the technique for how much the errors can be reduced, it was decided

not to include a parameter sweep. Instead, some parameters were tested and the best of those was selected.

It would be possible to produce a more accurate result by improving the following areas of the processing.

1. Noise filtering
2. Phase unwrapping
3. DEM
4. Atmosphere conditions
5. Other phase contributions

The Goldstein phase filter worked quite well, the interferogram became much less noisy but it could be possible to use even more filtering if the amount of noise causes problems for the phase unwrapping algorithm. If the phase unwrapping algorithm in SNAP is not good enough, other phase unwrapping algorithms could be tested.

The SRTM DEM was used in the 2-pass case. The SRTM DEM is one of the best freely available DEM:s, however, it is possible to purchase even more accurate DEM:s, thus it could be an option to pay to get a more accurate DEM over the area of interest. A drawback of that is if the area of interest is very large, then the cost could be very high and there might not exist very accurate DEM:s for large areas.

No atmospheric effects were assumed in the processing because that was the best guess based on the available information. If atmospheric data is collected for the time of the Sentinel-1 acquisition, a more sophisticated model can be made for the atmospheric effects. The other phase contributions and error could also be reduced by making models. However, since models also introduce errors it is important to be careful how they are created and be aware of how they are used.

The displacement graphs from the persistent scatterer technique also give some insight in the accuracy of 2-pass and 3-pass. The points in the graphs can be considered as 2-pass between one of the reference images and the master image. Even though the trend of a pixel shows for example a settlement, individual points in the graph can show both stability and uplift meaning that a 2-pass or 3-pass analysis can show either depending on the acquisitions. This is not only the case for the unreliable result from SNAP, but can also be seen in the result from SkyGeo who has actively removed errors and noise in the processing in both the TerraSAR and Sentinel case. This shows that even when there are models for error reduction in the processing, the results are unreliable for 2-pass and 3-pass. It is not known if the variations depend on noise and errors that are difficult to remove or if they depend on actual movement of the ground. In some cases, the magnitude of the movement appears unreasonably large so that it must depend on residual errors but if the results include actual short-term fluctuations it would be an interesting result.

5.2 Sentinel-1 in SNAP compared to results by SkyGeo

What the comparison between the results from the SNAP processing and the results provided by SkyGeo really gives is the comparison of the different processing procedures. Thus, the difference when a large effort is taken to remove errors (SkyGeo) and when most errors are neglected (processing in SNAP).

What becomes clear when looking at the graphs from the same time period between the different processing procedures is that the error handling is necessary in order to make a more reliable result. This is also confirmed when looking at the RMS errors. The RMS errors from the SNAP analysis are of a magnitude such that the results are deemed unreliable. However, when comparing the displacement maps from the SNAP processing in Figure 4.15 and the SkyGeo results in Figure 4.18 it can be seen that the results are similar with the exception of a bias in the SNAP processing. This bias or shift appear clearly when comparing the displacement rates along the tracks in Figures 4.25 and 4.26. The shift is probably caused by remaining errors that mistakenly appear as displacement. It is possible that the shift is caused by untreated atmospheric effects. Then, by using atmospheric data to create a model for atmospheric effects it may be possible to remove the shift and then the trend will appear similar to the other data. It appears probable that the offset is caused by untreated errors and uncertainties and thus error removal should reduce the shift or bias.

A potential issue with the comparison in Figures 4.25 and 4.26 is the difference in the time periods. The time periods of the SkyGeo stacks are roughly the same but shifted and the stack used for the SNAP processing is much shorter. For example, if an event occurred in early 2016, it will appear in the TerraSAR-X results but not in the others. In the same way, if an event occurred in 2019 it will appear only in the Sentinel by SkyGeo results. Further, because the SkyGeo stacks spans over several years, they include seasonal variations which are not present in the Sentinel in SNAP results. This causes an ambiguity in the comparison since it is not certain if differences come from the techniques and satellites or from different events. It is possible that the smooth curve from the SNAP processing is caused by the lack of seasonal variations present in the others and that the SNAP curve appear like the others if the time period spanned over several years. However, although there is an ambiguity in the graphs, Figures 4.25 and 4.26 give an idea of the differences between the different techniques and there is an overlap in time for all three graphs in the figure. Therefore, the figures can be used for comparison if the possible ambiguities are considered.

There are also areas in the displacement maps that have similar results without a bias which gives an indication that unwrapping errors and atmospheric effects may not affect all the measurements. Therefore, although the SNAP processing used is not completely reliable at this point it appears that it works to some extent and may be usable with some further steps for error removal.

5.3 TerraSAR-X compared to Sentinel-1

The comparison between the results from TerraSAR-X and Sentinel-1 provided by SkyGeo gives an idea of the differences between the satellites. The processing between them is the same and the time period is roughly equally long and during roughly the same time. Looking at the displacement maps for the total area for both cases the result looks very similar. Most pixels show similar displacement rates and the PSC are similar in both cases with the exception that the TerraSAR results have a more dense network of PSC caused by the higher spatial resolution.

The displacement graphs show that the measurements follow the trends clearly with the difference that the Sentinel results vary a little bit more. This can also be seen in the RMS error of the linear fit for the pixels. The RMS errors lie between 0.5 and 3.9 mm for TerraSAR-X and between 1.3 and 9.7 mm for Sentinel-1. Although larger errors for Sentinel-1, it is not unreasonably large and the results are still considered reliable.

It is interesting to find the correlation between high coherence and low RMS error and that the RMS errors appear to be well distributed over the error range. This implies that there is not a very good nor very bad pixel when calculating the RMS errors, but the errors are spread across the range given by the minimum and maximum value. The correlation between high coherence and low RMS value is also interesting. While high coherence is more often found for pixels located in urban areas, that is not necessarily always the case, and that means that low RMS errors can be found for other pixels as well. Since low RMS error implies a linear displacement in this case and low RMS error is correlated with high coherence, it is expected that a pixel with high coherence shows a vertical displacement with a linear movement in time regardless of the location. Pixels with high coherence should therefore be easy to anticipate how they will move in the future since they follow a linear trend. This should be considered with caution though. This result is based on measurements during a 3-year time period. It is not unlikely that an area changes velocity even though it has had the same velocity during this measurement period. Changes in the velocity can be caused by many factors and may occur. It is possible that there are pixels in the data set which have changed their velocity during the measurement period and those appear to have a larger RMS error since they will not fit well to a model with a single displacement rate. A thorough analysis of pixels changing velocity has not been done and therefore an absolute conclusion cannot be drawn. However it does seem plausible that a pixel with high coherence can be expected to have a linear displacement rate based on the analyzed data.

Lindome and Kållerød railway stations are analyzed further to find differences between the results. The displacement maps in Kållerød show similar results. The area that has a known displacement issue confirmed by Trafikverket and that can be seen with the naked eye is clearly red in both the measurements. The stable green points and the yellow points also coincides to a large extent in both images which implies that the same movement with a similar magnitude is detected with both TerraSAR-X and Sentinel-1. The only difference is that a few blue pixels can

be seen in the Sentinel-1 result which indicates uplift. No such pixels can be seen in the TerraSAR-X results. Since the blue pixels are so few and spread out, for example a single blue pixel can be found in an otherwise yellow area which means that the general movement can still be seen. Therefore this is not seen as an issue.

When looking at Lindome station, there are some larger differences. The aforementioned tunnel, clearly visible in the TerraSAR-X results as a line of green points across a red area is not that clear in the Sentinel-1 results. The PSC around the tunnel are more sparse as expected from the lower spatial resolution but the magnitude of the displacement rate is also different. The tunnel with several green (stable) points in the TerraSAR-X results is marked with a clear darkblue point (strong uplift) in the Sentinel-1 results. Further, the area north of the tunnel show similar results in both cases, but south of the tunnel the TerraSAR-X results show red points (strong settlements) while the Sentinel-1 results show yellow/orange points (settlements). With previous knowledge, the points of the Sentinel results show the issues around the tunnel, but it would be difficult to conclude that from just looking at the displacement map. In the displacement map from the TerraSAR results, it is obvious that the railway is settling around the stable tunnel, and that conclusion can almost be drawn directly from the displacement map without a visit to the area. Other than the tunnel and some points around the parking lot, the displacement maps agree over Lindome.

The similarities in the displacement maps appear also when looking at the displacement rates along the tracks in Figures 4.25 and 4.26. In the figures it can be seen however that although the trends are similar, there are small differences in the absolute values. Therefore, these measurements may not be reliable if an absolute value of the displacement rate is desired, but because of the similar trends they both appear reliable to highlight problematic areas.

5.4 InSAR and Optram

The railway measurements from Optram are relative measurements that give a standard deviation and a so-called b -value connected to the variations of the height measurements. Because of this, it is difficult to extract movement in mm/year from Optram and therefore it is difficult to compare the magnitude of Optram and InSAR. Instead, the measurements could compliment each other by indicating problem areas. For example, if the Optram result is compared to the displacement maps from TerraSAR-X and Sentinel-1 it can be seen that the settlement issues in Lindome and Källered is clear in all of the images. Then Optram sees more details on the track between the stations, an area where the InSAR results show green (stable) pixels. Therefore, the InSAR results can be used as an indication that the railway has potential issues in Lindome and Källered and a measurement train can be sent to the area to measure more carefully and report it to Optram. Maintenance work can then be decided on based on the results in Optram.

InSAR is not suitable to replace Optram. Partly because of the reasons mentioned

above, but also because the measurement trains measure the rails while the InSAR measurements measure the railway embankment and not only the rails. Therefore, InSAR cannot guarantee that the railway has a certain movement. Instead InSAR can highlight potential problem areas and give insight of the movement in the area. For example, if the data in Optram suggests that the railway is sinking it may actually be the entire area that is sinking. In that case, it is pointless to assign maintenance work to lift the rails because the ground will continue to sink. That information can be retrieved from the InSAR results.

5.5 Errors and noise

It is obvious from all the InSAR results that errors and noise are issues for the technique. Thorough processing to remove errors and noise is required in order to get reliable results but even then there are some residuals that can possibly affect the data. For example, all time series show some fluctuations. Also the Norwegian *InSAR Norway* project that also uses Sentinel-1 data has fluctuations in the data sets [23]. This is not an issue for the PSI technique since the trend is the most important part, but a deeper understanding of the fluctuation could improve the results. For example, are they a result of residual errors and noise and in that case what source is the strongest in the residual errors and how can that be removed? Theoretically, the ground may fluctuate a bit as well and seasonal change could possibly be detectable as well. If it is, then that would be valuable information as well.

An interesting development would be to place reference measurements at some pixels. For example GPS stations that could be used to measure the position of a pixel. Then fluctuations in the height direction can be compared for the InSAR and GPS measurements to give an idea if the major fluctuations come from noise sources and errors or if there may be changes in the soil that affect the results as well. In any case, the use of GPS stations would improve the understanding of InSAR measurements. For example, a couple of GPS receivers could be placed where there are PSC and collect data for another 2-3 years and then compare the data. Another positive aspect of using GPS is that the GPS measurements can be used to correct for atmospheric effects, which is already done at some locations. The GPS receiver should be an advanced receiver in order to make corrections of the atmosphere and to measure the height with enough accuracy.

6

Conclusions

In this chapter, the conclusions of the report are presented.

6.1 Intensity measurement

The intensity image created from the mean value of several shows that the railway gives a strong reflected signal over time. Although the intensity measurements cannot be used to draw conclusions about displacement, the strong intensity from the railway implies that the railway is a reliable scattering object that can give reliable displacement results. This means that the railway could possibly give stable reliable points in other areas outside the area used in this project.

6.2 Differential in SNAP

With some basic knowledge in InSAR theory, it was quite simple to create displacement maps from the Sentinel-1 data. The issue is that there are errors and uncertainties that cause the result to be unreasonable if mm accuracy is wanted. By using more data about atmospheric conditions at the time of the acquisitions, using a more accurate DEM, and developing better models for the remaining errors it might be possible to reduce the errors to a degree where the result is usable. The PSI analysis of the data processed by SkyGeo showed that even though many error sources were removed, the direction of the movement could still change depending on the acquisitions. Using a stack of images to reduce errors statistically in the PSI technique avoids the introduction of model errors and is therefore a better way to reduce the errors if the models are not accurate. Hence, it is not recommended to use the DInSAR technique for railway deformation monitoring.

6.3 Persistent scatterer

The persistent scatterer technique for InSAR processing seems to work well. After removing error sources in the processing, both the results from the TerraSAR-X and

Sentinel-1 data showed promising results with the exception for the tunnel in Lindome in the Sentinel-1 data. It is difficult to make definitive conclusions regarding the future use of InSAR for railway measurements and whether the Sentinel-1 data is reliable enough. This is more of a feasibility study, a first step in the analysis of whether InSAR is a reliable way of measuring deformations. The definitive conclusions that can be drawn about the PSI technique is that the error sources like for example atmospheric effects must be considered and removed in order to get reliable results which was clear from the processing in SNAP. With that said, SNAP proved to be a powerful tool in the InSAR processing and may be used, but models for error removal should be applied in post processing.

It seems possible that the Sentinel-1 data is good enough based on the results in this project. Except for the tunnel, the Sentinel data shows results similar to the results from the TerraSAR-X data. The tunnel data from Sentinel was not completely wrong either, it was just not as clear as the results from TerraSAR-X. Since the RMS errors were relatively low and the data followed the linear trends well it seems plausible that Sentinel-1 can be used for this type of reliable measurement. However, when analyzing the displacement maps one should be aware that cases like the Lindome tunnel may occur and that even early warning signs should be taken seriously. Based on that and the fact that the displacement maps from both satellite constellations missed some movement detected in the Optram data, it is concluded that InSAR cannot replace the measurement trains and Optram system at this point. InSAR can just act as a valuable complimentary system that can highlight areas that should be investigated further. InSAR can also help with the understanding of how a larger area and how the soil is moving in a way that the Optram data cannot.

Noise and error sources are issues for the InSAR measurements. In this feasibility study, the Sentinel-1 data would be possible to use to create displacement maps but a deeper understanding of residual errors and ground fluctuations may be desired before making a final decision. A future study with reference measurements with for example GPS may give a deeper understanding of how the ground is changing and how much residual errors there is in the processed InSAR data. With a deeper understanding and if further error removal is possible, DInSAR may serve as an excellent way of measuring short term movement, but that is not the case now.

The area of interest used in the study was chosen because there are known displacement issues, it was easily accessible, and there are lots of other data and knowledge about the area. While it has a mixed nature with urban areas, roads, railway, lakes, forests, etc. it does not cover all nature types in Sweden. It can be shown that PSI works well in urban areas, for the railway, and for some other places where there happen to be a well scattering object but other nature types should be examined further before making a decision of creating nationwide displacement maps. For example mountainous areas or places where the railway is surrounded by dense vegetation may introduce more errors or decrease the number of PSC.

The conclusion that can be drawn is that InSAR, and more precisely persistent scatterer with Sentinel-1 data is plausible to use for deformation maps, but further studies are required in order to make the results more reliable. For areas similar to

the Lindome and Kållerød areas, it could possibly be used as it is right now. However, more knowledge is needed, for example about the residual noise, and questions like how different nature types affect the results, can measurements give reliable results during winter and snow need to be answered through further research to make the results more reliable. Also, research on how the processes used in this study could be more efficient could improve the reliability of the results. The many variables that can be changed during the processing and many different functions that can be used can surely be improved, and through research on how to optimize the processing an even better result can possibly be created. However, given the many parameters, such a project would require a large amount of time.

Bibliography

- [1] Trafikverket. *Sättningar*. URL: <https://www.trafikverket.se/nara-dig/Vastra-gotaland/projekt-i-vastra-gotalands-lan/Vastlanken---smidigare-pendling-och-effektivare-trafik/Vastlankens-miljoarbete/fakta-om-sattningar/> (visited on 04/29/2019).
- [2] S. Barthelemy, J. Spännar, and O. Åkergren. *Optram Användarmanual*. Trafikverket. July 2018.
- [3] S. Wahlund et al. *Mätmetoder för sättningsmätning, en utvärdering av traditionell avvägning och dInSAR*. Tech. rep. Kruthusgatan 17, 411 04 Gothenburg: Trafikverket, Aug. 2017.
- [4] K. Zalite and K. Voormansik. *Differential and Persistent Scatterer SAR Interferometry .. DInSAR & PS-InSAR*. Tech. rep. Tartu Observatory, June 2016.
- [5] W.G. Rees. *Physical principles of remote sensing*. 3rd ed. University Printing House, Cambridge CB2 8BS, United Kingdom: Cambridge university press, 2013. ISBN: 978-0-521-18116-7.
- [6] Roger J. Sullivan. *Radar foundations for imaging and advanced concepts. [electronic resource]*. SciTech Pub., 2004. ISBN: 1891121227. URL: <http://proxy.lib.chalmers.se/login?url=http://search.ebscohost.com.proxy.lib.chalmers.se/login.aspx?direct=true&db=cat06296a&AN=clc.b2001183&site=eds-live&scope=site>.
- [7] European Space Agency. *SAR Applications*. URL: <https://earth.esa.int/web/guest/-/sar-applications-4019> (visited on 04/29/2019).
- [8] W. Keydel. “Normal and Differential SAR Interferometry”. In: *Educational Notes RTO-EN-SET-081bis 2* (2007),
- [9] R. Bamler and P. Hartl. “Synthetic aperture radar interferometry”. In: *Inverse Problems* 14 (Feb. 1998), R1–R54.
- [10] P. A. Rosen et al. “Normal and Differential SAR Interferometry”. In: *Educational Notes RTO-EN-SET-081bis 2* (2007),
- [11] European Space Agency. *Sentinel-1*. URL: <https://sentinel.esa.int/web/sentinel/missions/sentinel-1> (visited on 04/29/2019).
- [12] L. Veci. *S1TBX TOPSAR Interferometry with Sentinel-1 Tutorial*. European Space Agency. Aug. 2016.
- [13] A. Ferretti et al. *InSAR Principles: Guidelines for SAR Interferometry Processing and Interpretation (TM-19)*. ESTEC, Postbus 299, 2200 AG Noordwijk, The Netherlands: ESA Publications, Feb. 2007. ISBN: 92-9092-233-8.

- [14] *Sentinel-1 processing with GAMMA software*. Gamma Remote Sensing. Worbsstrasse 225, CH-3073 Gümligen, Switzerland, Dec. 2017.
- [15] R. Bamler et al. “SRTM and beyond: Current situation and new developments in spaceborne InSAR”. In: (Jan. 2003).
- [16] Sang-Eun Park. “Variations of Microwave Scattering Properties by Seasonal Freeze/Thaw Transition in the Permafrost Active Layer Observed by ALOS PALSAR Polarimetric Data”. In: *Remote Sensing* 7 (Dec. 2015), pp. 17135–17148. DOI: 10.3390/rs71215874.
- [17] U.S. Geological Survey. *What are digital elevation models (DEMs)?* URL: <https://www.usgs.gov/faqs/what-are-digital-elevation-models-dems> (visited on 04/29/2019).
- [18] Lantmäteriet. *Elevation data, grid 2+*. URL: <https://www.lantmateriet.se/en/maps-and-geographic-information/geodataprodukter/hojddata-grid-2/> (visited on 06/05/2019).
- [19] NASA. *Shuttle Radar Topography Mission*. URL: <https://www2.jpl.nasa.gov/srtm/mission.htm> (visited on 04/29/2019).
- [20] CGIR CSI. *SRTM 90m DEM Digital Elevation Database*. URL: <http://srtm.csi.cgiar.org> (visited on 04/29/2019).
- [21] Alaska Satellite Facility. *Create a Sentinel-1 DEM*. URL: <https://www.asf.alaska.edu/asf-tutorials/data-recipes/create-a-sentinel-1-dem/> (visited on 04/29/2019).
- [22] A. Ferretti, C. Prati, and F. Rocca. “Permanent Scatterers in SAR Interferometry”. In: *IEEE Transactions on geoscience and remote sensing* 39.1 (Jan. 2001).
- [23] Geological Survey of Norway. *InSAR Norway*. URL: <https://insar.ngu.no> (visited on 04/29/2019).
- [24] Geological Survey of Norway. *InSAR Norway: About the mapping service*. URL: <https://www.ngu.no/en/topic/about-mapping-service> (visited on 04/29/2019).
- [25] Copernicus Open Access Hub. URL: <https://scihub.copernicus.eu/dhus/#/home> (visited on 04/29/2019).
- [26] Stanford Radar Interferometry Research Group. *SNAPHU: Statistical-Cost, Network-Flow Algorithm for Phase Unwrapping*. URL: <https://web.stanford.edu/group/radar/softwareandlinks/sw/snaphu/> (visited on 06/10/2019).
- [27] F.J. Van Leijen. “Persistent Scatterer Interferometry based on geodetic estimation theory”. PhD thesis. Delft University of Technology, 2014.
- [28] Infranord. *Maskinell tillståndsbedömning*. URL: http://www.infranord.se/media/2589/maskinell_tillstaandsbedoemning_infranord_120411.pdf (visited on 06/10/2019).
- [29] Trafikverket. *Koll på spåret i 200 km/tim*. URL: <https://www.trafikverket.se/tjanster/system-och-verktyg/forvaltning-och-underhall/Periodiskmatning/Spar-och-kontaktledningsmatningar/Koll-pa-sparet-i-200-kmtim/> (visited on 06/10/2019).